

1967

Bremsstrahlung Production in Thick Germanium Targets

Harold R. Compton

College of William & Mary - Arts & Sciences

Follow this and additional works at: <https://scholarworks.wm.edu/etd>



Part of the [Physics Commons](#)

Recommended Citation

Compton, Harold R., "Bremsstrahlung Production in Thick Germanium Targets" (1967). *Dissertations, Theses, and Masters Projects*. Paper 1539624631.

<https://dx.doi.org/doi:10.21220/s2-rwn4-nn85>

This Thesis is brought to you for free and open access by the Theses, Dissertations, & Master Projects at W&M ScholarWorks. It has been accepted for inclusion in Dissertations, Theses, and Masters Projects by an authorized administrator of W&M ScholarWorks. For more information, please contact scholarworks@wm.edu.

BREMSSTRAHLUNG PRODUCTION IN THICK GERMANIUM TARGETS

A Thesis

Presented to

The Faculty of the Department of Physics
The College of William and Mary in Virginia

In Partial Fulfillment
Of the Requirements for the Degree of
Master of Arts

By

Harold Randolph Compton

August 1967

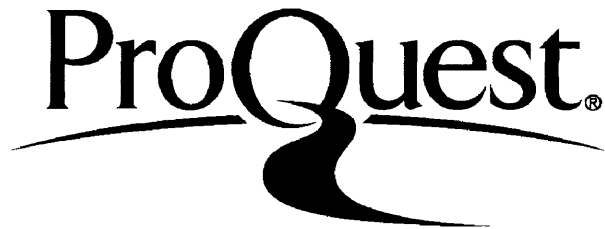
ProQuest Number: 10625038

All rights reserved

INFORMATION TO ALL USERS

The quality of this reproduction is dependent upon the quality of the copy submitted.

In the unlikely event that the author did not send a complete manuscript and there are missing pages, these will be noted. Also, if material had to be removed, a note will indicate the deletion.



ProQuest 10625038

Published by ProQuest LLC (2017). Copyright of the Dissertation is held by the Author.


All rights reserved.

This work is protected against unauthorized copying under Title 17, United States Code
Microform Edition © ProQuest LLC.

ProQuest LLC.
789 East Eisenhower Parkway
P.O. Box 1346
Ann Arbor, MI 48106 - 1346


APPROVAL SHEET

This thesis is submitted in partial fulfillment of
the requirements for the degree of
Master of Arts

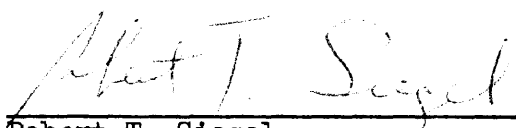


Author

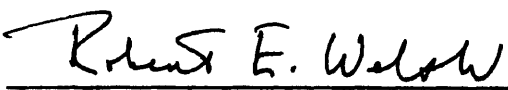
Approved, August 1967:



Morton Eckhause



Robert T. Siegel



Robert E. Welsh

ACKNOWLEDGMENTS

The experiment reported in this paper was authorized by the NASA, Langley Research Center, Hampton, Virginia, under the supervision of Dr. Jag J. Singh. The author is grateful to the Langley Research Center for its endorsement, and especially to Dr. Jag J. Singh for his constructive criticism.

TABLE OF CONTENTS

	Page
ACKNOWLEDGMENTS	iii
LIST OF FIGURES	v
ABSTRACT	vii
INTRODUCTION	2
Chapter	
I. BREMSSTRAHLUNG THEORY AND DISCUSSION	5
Historical	5
General Discussion	5
Theoretical Cross Sections	9
Bremsstrahlung Spatial Distribution	11
Bremsstrahlung Efficiency	13
II. EXPERIMENTAL APPARATUS AND METHOD	14
Apparatus Arrangement	14
Target Chamber	15
Target Material and Thickness	16
Detectors	16
Analyzer	17
Current Integrators	17
Experimental Method	18
III. CORRECTIONS TO EXPERIMENTAL DATA	20
IV. RESULTS AND DISCUSSION	25
Bremsstrahlung Intensity	25
Angular Distribution	25
Efficiency of Production	27
Differential Cross Section	27
V. CONCLUDING REMARKS	30
REFERENCES	31
VITA	32

LIST OF FIGURES

Figure	Page
1. Arrangement of experimental equipment	33
(a) View from above	33
(b) View from right side	34
(c) View from left side	35
2. Schematic of detection arrangement. The angle θ is measured from the forward direction of the incident electron beam to the target-detector line with 0° being in the forward direction	36
3. Typical spectrum from calibration source Na^{22} (0.511 MeV and 1.28 MeV)	37
4. Typical spectrum from calibration source Cs^{137} (0.667 MeV)	38
5. Typical spectrum from calibration source Co^{60} (1.17 MeV and 1.33 MeV)	39
6. Typical pulse height analyzer calibration curve	40
7. Typical bremsstrahlung spectrum in the photon energy range 0.38 MeV to 1.0 MeV before any corrections ($\theta = 60^\circ$). Incident electron energy $E_0 = 1.0$ MeV . . .	41
8. Typical bremsstrahlung spectrum in the photon energy range 0.38 MeV to 1.0 MeV before any corrections ($\theta = 120^\circ$). Incident electron energy $E_0 = 1.0$ MeV . . .	42
9. Detector efficiency	43
10. Photon or bremsstrahlung intensity for several energy ranges. The curves for the energy ranges 0.63 MeV to 0.78 MeV and 0.83 MeV to 1.0 MeV have been adjusted so that they have the same values as that for 0.38 MeV to 0.58 MeV at $\theta = 15^\circ$. Incident electron energy $E_0 = 1.0$ MeV	44

Figure	Page
11. Angular distribution of total radiated intensity ($I(\theta)$) for photon energy range from 0.38 MeV to 1.0 MeV. Incident electron energy $E_0 = 1.0$ MeV	45
12. Comparison of experimental bremsstrahlung differential cross section $\frac{d\sigma}{dk d\theta}$ with the Born-approximation cross section. Incident electron energy $E_0 = 1.0$ MeV	46
(a) $\theta = 15^\circ$	46
(b) $\theta = 30^\circ$	47
(c) $\theta = 45^\circ$	48
(d) $\theta = 60^\circ$	49
(e) $\theta = 75^\circ$	50
(f) $\theta = 90^\circ$	51
(g) $\theta = 105^\circ$	52
(h) $\theta = 120^\circ$	53
(i) $\theta = 135^\circ$	54
13. Peaking of the bremsstrahlung cross section $\frac{d\sigma}{dk d\theta}$ in the forward direction. Incident electron energy $E_0 = 1.0$ MeV	55
14. Comparison of experimental bremsstrahlung cross section $\frac{d\sigma}{dk}$ with Born-approximation cross section. Incident electron energy $E_0 = 1.0$ MeV	56

ABSTRACT

An experiment was performed at the Langley Research Center, Hampton, Virginia, in which bremsstrahlung radiation in the energy range from about 0.38 MeV to 1.0 MeV was measured when thick germanium targets were bombarded by 1.0 MeV electrons. The experimental angular distribution of the bremsstrahlung intensity, $I(\theta)$, along with the differential cross sections $\frac{d\sigma}{dkd\theta}$ and $\frac{d\sigma}{dk}$ are presented and compared with theoretical calculations. The efficiency of photon production is also compared with theoretical calculations. As expected, the intensity decreases as the angle between the incident electrons and the emergent photon increases and as the photon energy increases.

BREMSSTRAHLUNG PRODUCTION IN THICK GERMANIUM TARGETS

INTRODUCTION

Future space flights may include vehicles traveling through regions of highly concentrated energetic particles trapped in the earth's magnetic field. Electrons constitute a large portion of these charged particles (ref. 1) and it is well known that when electrons pass through matter they lose kinetic energy through the processes of excitation and ionization and radiative emission in the electric field of the atomic nucleus and electrons. In the case of high energy electrons the most prominent energy loss is that due to radiation in the electric field of the nucleus. The radiation emitted by the electron in this process is due to the acceleration of the electron by the coulomb field of the nuclei of the stopping material. This radiation is referred to as bremsstrahlung and it is this process of bremsstrahlung production with which this investigation is concerned. Because of the presence of energetic particles in space, measurements are needed for such things as estimation of radiation doses inside space vehicles for biological purposes and the determination of the effects of radiation on the vehicle's skin and instruments.

Numerous investigations of bremsstrahlung production are reported in the literature for the case of nonrelativistic electrons, both experimental and theoretical. However, in the intermediate energy range where the kinetic energy of the electron is comparable to its rest energy the literature is not as complete and discrepancies in

experimental data with theoretical estimates are noted (ref. 2). Much of the thick target bremsstrahlung theory is based on thin target theory and information because of the lack of knowledge of electron scattering cross sections and cross sections for energy loss by various means in the thick target. In most practical situations the stopping material is thick and hence, because of inadequate theories, direct measurements of the bremsstrahlung is desirable.

Because of the hazards of bremsstrahlung which may be encountered in space flight and the lack of literature on thick target bremsstrahlung production, an experiment was performed at the Langley Research Center to measure the bremsstrahlung produced when a thick germanium target was bombarded with 1.0 MeV electrons. The target was sufficient thickness to cause the electrons to lose all their kinetic energy in traversing the target. This experiment is one of a series which was performed to determine bremsstrahlung production as a function of the target material and the incident electron energies. In this experiment the bremsstrahlung spectra were accumulated for angles varying from 15° to 135° with respect to the incident electron beam, which was always normal to the target.

The spectra, after appropriate corrections, were used to calculate the efficiency of production, various cross sections, and the angular distribution of the radiated energy over a photon energy range of about 0.4 MeV to 1.0 MeV. Comparisons have been made with the predictions of the Bethe-Heitler theory which show that the experimental results are in

reasonable agreement with the theoretical calculations. Direct comparison with theory was not possible since no comprehensive theory has been developed for thick target X-ray production.

CHAPTER I

BREMSSTRAHLUNG THEORY AND DISCUSSION

Historical

In 1895 Roentgen accidentally discovered X-rays through their ability to fluoresce certain salts of heavy metals after having passed through several millimeters thickness of optically opaque material. At the time Roentgen was studying electrical discharges in gases and he immediately began a study of the new radiation. From these first observations, many of the fundamental properties of X-rays were established and were later confirmed by other investigators whose research helped extend them. In particular, it was found that the X-rays consisted of a continuous spectrum, called bremsstrahlung, upon which was superimposed a line spectrum, or characteristic spectrum. The continuous spectra were identified and associated with the deflection of incident charged particles by the coulomb fields of the nuclei whereas the characteristic spectra have been identified with the electromagnetic radiation given off by an atom as it fills vacancies in electronic states.

General Discussion

When passing through matter, electrons lose their kinetic energy or they are deflected from their original path through inelastic and elastic collisions with the atomic nuclei and electrons. In the elastic

collisions the incident electrons may be deflected, however, no electromagnetic radiation is emitted by the incident electrons. For the case of inelastic collisions with the atomic nuclei the incident electron is deflected from its original path and emits radiation. As stated earlier, it is this particular mechanism of radiation production with which this investigation is concerned.

Although it was desired to measure the bremsstrahlung directly in this experiment, part of the radiation reaching the detector was due to the characteristic or line spectrum of the germanium target. However, the highest energy in this discrete spectrum was much less than the lowest energy considered in this investigation and hence this characteristic spectrum was ignored. Electron-electron bremsstrahlung was also ignored since, according to reference 3, it is expected to constitute no more than 3 percent of the total bremsstrahlung radiation.

In accord with classical theory, it is expected that whenever a charged particle is accelerated it will radiate and hence an electron which experiences a collision with the atomic nucleus should emit electromagnetic radiation whose amplitude is proportional to the acceleration. This acceleration is proportional to $\frac{Ze^2}{m}$ where Z is the atomic number of the nucleus, e is the electronic charge, and m the electron mass. Therefore the intensity which is proportional to the square of the amplitude varies as $\frac{Z^2}{m^2}$. Thus the total bremsstrahlung per atom varies as the square of the atomic number and inversely with the mass of the electron. Hence it is expected, due to the small mass of the electrons, that radiative losses from electrons are much larger

than for the heavier particles such as protons. Indeed it is found that for most high-velocity particles bremsstrahlung is appreciable only for electrons.

Bethe and Heitler (ref. 4) have given a quantum-mechanical treatment of the energy loss of an electron by radiative collisions. They use the Dirac equation for the electron and the Born approximation, $\frac{Z}{137\beta} \ll 1$, to treat the electron-nucleus interaction. They calculate the cross section for the probability of an electron of incident energy E_0 emitting radiation with frequency between ν and $\nu + d\nu$. This probability has a strong dependence on the effective distance of the electron from the nucleus. This effective distance for bremsstrahlung is given in reference 3 as \hbar/q where q is the recoil momentum given to the atom in the process. The screening effect of the atomic electrons may be ignored if \hbar/q is small compared to the atomic radius and the electric field in which the electron radiates is essentially the coulomb field of the nucleus. An effective screening parameter (ref. 3) is given as

$$\gamma = \frac{100 mc^2 h\nu}{E_0 EZ^{1/3}}$$

where E_0 and E are the initial and final energy of the electron, mc^2 is the rest mass energy of the electron, Z is the atomic number of the target nuclei and $h\nu$ is the energy emitted. According to the statistical model of Fermi and Thomas, γ is essentially the atomic

radius divided by the effective distance parameter \hbar/q . If γ is very much larger than 1 screening may be neglected, however, for $\gamma = 0$, screening is complete. Since $\gamma \approx 10$ for this investigation, no screening was considered. Also, if \hbar/q is large compared to the nuclear radius then the charge distribution in the nucleus can be ignored and the assumption of a point charge can be made. This assumption is valid for the bremsstrahlung process (ref. 5).

For the case of no screening, $\gamma \gg 1$, Sauter calculated the cross section for the production of a photon in the frequency range $d\nu$ by an incident electron of energy E_0 (ref. 3). Bethe and Heitler also give similar results for $\gamma \gg 1$, along with the cases of partial and complete screening. It was found for the average overall collisions, that the classical and quantum-mechanical cross sections are of the same order of magnitude, namely,

$$\sigma_{\text{rad}} \sim \frac{Z^2}{137} \left(\frac{e^2}{m_0 c^2} \right)^2 \frac{\text{cm}^2}{\text{nucleus}}$$

even though the classical theory of bremsstrahlung incorrectly predicts the emission of radiation in every collision in which an electron is deflected. The quantum-mechanical treatment states that there is a finite probability that a photon will be emitted each time a particle suffers a deflection; however, this probability is very very small and usually no photon is emitted. In the few collisions where photons are

emitted, very large amounts of energy are radiated. Hence quantum mechanics allow for a small number of radiative collisions with large energy losses whereas classical mechanics allow for a multitude of radiative collisions with small energy losses. In this way the averages are about the same for the two theories. The spectral distributions are very different for the two theories and most experimental results are in reasonable agreement with the quantum-mechanical treatment.

Theoretical Cross Sections

Numerous bremsstrahlung cross sections have been derived by various investigators. These cross sections have been derived on the basis of whether or not the energetic particle is relativistic or nonrelativistic and from various assumptions about the effects of electron screening. Also various approximations, such as the Born approximation, are used in the derivation of these cross sections. Koch and Motz have given a very complete and integrated summary of the various cross sections in one paper (ref. 2). In their paper the cross section $d\sigma$, the transition probability per atom per electron divided by the incoming electron velocity, is given for single photon emission in a large cubic box of sides L .

$$d\sigma = \frac{w}{(p_0 c / E_0)} \left(\frac{\hbar}{m_0 c} \right)^3 L^3$$

where

$$w = (2\pi/\hbar)\rho_f |H_{if}|^2$$

The factor ρ_f is the density of the final state and is written as

$$\rho_f = \frac{pEk^2 dk d\Omega_k d\Omega_p L^6}{(2\pi)^6 m_0 c^2}$$

H_{if} is an element of the matrix for the transition of the system from an initial state before photon emission to a final state after the emission.

$$|H_{if}|^2 = \left(\frac{2\pi e^2}{\hbar c}\right) (m_0 c^2)^2 \left| \int \psi_f^* (\vec{\lambda} \cdot \vec{\alpha}) e^{-\vec{k} \cdot \vec{r}} \psi_i d\tau \right|^2 L^{-9}$$

The expressions for $d\sigma$, w , ρ_f , and $|H_{if}|^2$ have been taken directly from reference 2 and the reader is referred to this paper for the terminology used. However, it should be noted that the important and perhaps the most difficult quantity to be evaluated is the matrix element H_{if} . In particular it is difficult to find the exact wave functions ψ_i and ψ_f , Dirac wave functions for the initial and final electrons, which describe an electron in a screened, nuclear coulomb field. The solution to the Dirac wave equation cannot be given in closed form but must be represented by an infinite series. Hence various approximate wave functions and procedures have been used.

Koch and Motz emphasize the Born approximation cross-section formulas in their paper because these formulas have been fairly successful in predicting the properties of the bremsstrahlung radiation. The approximation assumes $\frac{Z}{137\beta} \ll 1$ and free particle wave functions perturbed to first order in Z . Two of the bremsstrahlung cross sections using the Born approximation and the assumption of an unscreened nuclear coulomb field are given in formulas 2BN and 3BN (ref. 2). Formula 2BN is differential in photon energy and emission angle whereas formula 3BN is differential in photon energy only. These cross sections are of interest for the theoretical comparisons made in this investigation and are given in reference 6 (with some rearrangement of terms), in the form in which they were used in a computer program.

Bremsstrahlung Spatial Distribution

It was stated earlier that the spectral distribution obtained from classical considerations was very different from the quantum-mechanical treatment and in general the experimental results were in reasonable agreement with quantum mechanics. Therefore the emphasis here is on the quantum-mechanical calculation of the bremsstrahlung spectrum. The Born approximation theory becomes less reliable as the atomic number of the target increases, the initial electron energy decreases, and the photon energy approaches the high frequency limit. However, for cases where the Born approximation breaks down the cross sections are reasonably good and may be expected to give at least the correct order of magnitude (ref. 2). It should also be pointed out that the cross

sections discussed in the previous section, formulas $2BN$ and $3BN$, are for the case of a single electron incident normal to a thin target in which the electron collides with an atom and emits a photon upon deflection from its original path. However, this is not the true picture for thick-target calculations because of the electron's straggling as it passes through the target. Before coming to rest in the target, the electron may suffer many deflective collisions in which photons may or may not be emitted. There is an uncertainty of the amount of energy loss as the electron traverses the thick target and the absorption and attenuation of the X-ray in the target must be considered. Therefore, in order to make more accurate calculations of the bremsstrahlung spectrum a better physical model of the actual situation must be established. One such model from which theoretical values have been obtained has been constructed and programmed for the IBM 7094 digital computer at the Langley Research Center.*

The model which was programmed is explained in detail in Chapter II reference 6. In general the thick target is approximated by a laminar structure of thin targets in which there are equal energy losses by the electron. The assumptions were made that an incident electron of energy E_0 passed through the laminated target strips with equal energy losses in each strip and that the energy loss was due to collisions with atomic electrons only. The assumption of energy loss due to atomic electrons

*The theoretical model was programmed and the results were provided by Chris Gross, NASA, Langley Research Center, Hampton, Virginia.

only is valid for electron energies of 1 MeV or less. The electron passed through the energy range of E_0 to 0 and came to rest in the target. In order to calculate $\frac{d\sigma}{dk d\theta}$ it was necessary to determine the angular distribution of the electron intensity as the electrons passed through the thick laminated target. This was done by using the Goudsmit-Saunders theory (ref. 7) and, in particular, their angular distribution formula for multiple scattering deflections as given in reference 8.

After calculating $\frac{d\sigma}{dk d\theta}$ the bremsstrahlung intensity of energy k at an emission angle θ , $I(\theta, k)$, was calculated from

$$I(\theta, k) = \int_0^E \int_0^\pi \int_0^{2\pi} N(E) A_{GS}(\eta) \left(\frac{d\sigma}{dk d\theta} \right) e^{-\frac{\mu(k)t}{2 \cos \theta}} d\phi d\eta dE \quad (1)$$

where $A_{GS}(\eta)$ is the electron intensity in the direction of η ; $N(E)$ the number of atoms which may be encountered by an electron of energy E ; $\frac{d\sigma}{dk d\theta}$ the Bethe-Heitler bremsstrahlung cross section; $\mu(k)$ the target absorption coefficient for bremsstrahlung of energy k , t the target thickness and ϕ the azimuthal angle.

Bremsstrahlung Efficiency

The bremsstrahlung efficiency, which is defined to be the ratio of the total radiated energy to the incident energy, was calculated using the above expression for $I(\theta, k)$ integrated over all space and photon energies.

CHAPTER II

EXPERIMENTAL APPARATUS AND METHOD

Apparatus Arrangement

The arrangement of the experimental equipment is shown in the photographs of figure 1 and the sketch in figure 2. A collimating beam tube assembly was attached to the Dynamitron accelerator and the target chamber was mated to the end of this beam tube assembly with a lucite insulator. The target chamber itself was mounted at the center of a circular table which was calibrated in 0.5° divisions from 0° to 360° . This calibration was used in the angular adjustments of the detector. The target was mounted inside the target chamber normal to the electron beam and was insulated from the target chamber. The bremsstrahlung detector was a 2-inch by 2-inch NaI(Tl) crystal mounted on a Dumont 6292 photomultiplier tube. This detector was located inside a lead cylinder which was mounted on top of a mobile platform. An aluminum arm extending from the center of the target chamber to the face of the cylinder was mounted so that it could rotate from 0° to approximately 180° along with the mobile platform. A line scribed on this aluminum arm from the center of the target chamber was used to set the detector at the desired angle and height. Another detector exactly like the one mounted on the mobile platform was fixed on the table at approximately 60° from the beam line on the side opposite to the scanning detector and it was shielded with lead bricks. This detector

remained fixed throughout the experiment and is referred to later as the monitor detector. Diffusion pumps were attached to the beam tube and target chamber assembly and were used to evacuate this assembly to a pressure of approximately 3×10^{-6} millimeters of mercury. Valves were placed appropriately in this assembly to allow the removal of a target without opening the entire beam tube to atmospheric pressure. A tripod-mounted TV camera was used to view the experimental equipment from the control console.

The arrangement and use of the peripheral electronic equipment used in this experiment are described in separate paragraphs of this chapter.

Target Chamber

The target chamber was a brass cylinder 8 inches in diameter with a quartz top. The top was designed so as to allow the raising or lowering of the target without breaking the vacuum in the chamber. Portholes were cut at intervals from 15° to 135° around the chamber to minimize attenuation of the bremsstrahlung. The thickness of the brass walls at each port was 0.079 centimeters. A cylindrical collimator used for mating to the beam tube collimator was brazed onto the front wall of the chamber. A small shaft was inserted through the chamber walls near the base of the chamber. This shaft was rigged to hold a simulated target and was connected to an external electric motor. This mechanism was used to raise or lower the simulated target from the control console.

Target Material and Thickness

Circular germanium targets 1 inch in diameter and 0.0844 cm thick were cut and prepared by the shop and laboratory in the Instrument Research Division at Langley. The thickness of each target was equal to the range of 1 MeV electrons in germanium plus 10 percent where the range is defined as the thickness of an absorber which the particle can just penetrate. The range was calculated from the equation given by Katz and Penfold (ref. 9) and is as follows:

$$R(\text{mg}/\text{cm}^2) = 412 E^n$$

where $n = (1.265 - 0.0954 \ln E)$ and E is the kinetic energy of the electrons in MeV.

Detectors

There were two detectors used in this experiment both of which were 2-inch by 2-inch NaI(Tl) crystals mounted on Dumont 6292 photo-multiplier tubes. One was a movable detector which was used to detect the spectrum at the various angles and the other was fixed on the table and was used to monitor the experiment. The face of each crystal had a protective covering of aluminum 0.08 cm thick.

The movable detector was located inside a lead cylinder which had a face thickness of 6 inches and a wall thickness of 3 inches. The diameter of the aperture in the cylinder at the face of the crystal was 0.625 inch. This detector was always located at a radial distance of

42 inches from the center of the target chamber. The output signal of this detector was suitably amplified and then fed into a 400-channel pulse height analyzer (TMC model 402).

The monitor detector was fixed on the table at approximately 12 inches from the center of the target chamber and at an angle of 60° on the side of the beam opposite to that scanned by the movable detector. A lead collimator was placed in front of this detector and it was then surrounded with lead bricks. The output of this detector was amplified and fed into a scaler which gave a visual display at any time during the experiment of the number of photons having reached this detector. This detector was used primarily to monitor fluctuations in the electron beam.

Analyzer

The spectrum detected at each angle was fed into the pulse height analyzer. The analyzer was calibrated using gamma ray sources of known accuracy and typical spectra of the known sources are presented in figures 3, 4, and 5. The calibration sources with discrete gamma are Na^{22} (0.51 and 1.28 MeV), Cs^{137} (0.667 MeV), and Co^{60} (1.17 and 1.35 MeV). The calibration curve is given in figure 6.

Current Integrators

The current incident on the target and the chamber was integrated with Elcor 309B current integrators to obtain the total charge deposited on the target and the chamber during any given run.

Experimental Method

The detection of the X-ray spectrum at a given angle is hereinafter called a run. Before making any detection runs it was necessary to make simulated runs in order to focus and adjust the beam to obtain a reasonable beam spot size and to make sure that the beam was incident on the target. The spot size was obtained by making PVC patterns. In this procedure the beam was focused on a piece of plastic and, due to the intensity of the beam, a smudge equivalent to the beam spot size was left on the plastic. This smudge was observed and the process repeated until the desired spot size was obtained. After obtaining the spot size it was necessary to adjust the beam to insure that it impinged upon the target. To do this a simulated target of titanium coated with zinc sulfide was inserted in the target chamber at the desired target location. When the electron beam hit such a target, the zinc sulfide would fluoresce and with the aid of the TV camera one could observe the beam pattern on the simulated target. The simulated target was moved out of the beam after proper beam adjustment and the germanium target was lowered into its place.

The germanium target was inserted into the target chamber so that it was normal to the incident electron beam. The movable detector was placed at the desired angle and then the Dynamitron accelerator was turned on and adjusted to produce a beam of monoenergetic 1 MeV electrons with a beam current of 2 nanoamperes. The length of a given run was equal to the time it took to obtain a preset number of counts from the monitor detector. At the beginning and end of each run pertinent

data were recorded from the control console and auxiliary electronic equipment. The spectrum obtained at each angle was fed into the pulse height analyzer and printed out on an IBM typewriter. The X-ray spectrum from the thick germanium target was measured at angles of 15° , 30° , 45° , 60° , 75° , 90° , 105° , 120° , and 135° .

In any experiment of this type there will be a certain amount of radiation reaching the detector which was not created at the target. Such radiation can be created by back-scattered electrons. This background must be accounted for in the actual spectrum. To do this the above process was repeated at each angle with the target completely removed from the target chamber. After appropriate corrections, which are explained in the next chapter, the spectra obtained at the various angles were subtracted from the initial spectra obtained with the target in place. The length of each background run was equal to the time it took to accumulate a charge on the chamber equal to the average of the total chamber and target charge in the initial runs.

Typical spectra obtained at the various angles are shown in figures 7 and 8. Also shown in the figures are the background spectra obtained at the same angles. No corrections have been applied to these spectra. The higher channel numbers correspond to the high energy end of the spectrum and one can note the expected decrease in intensity as the energy increases.

CHAPTER III

CORRECTIONS TO EXPERIMENTAL DATA

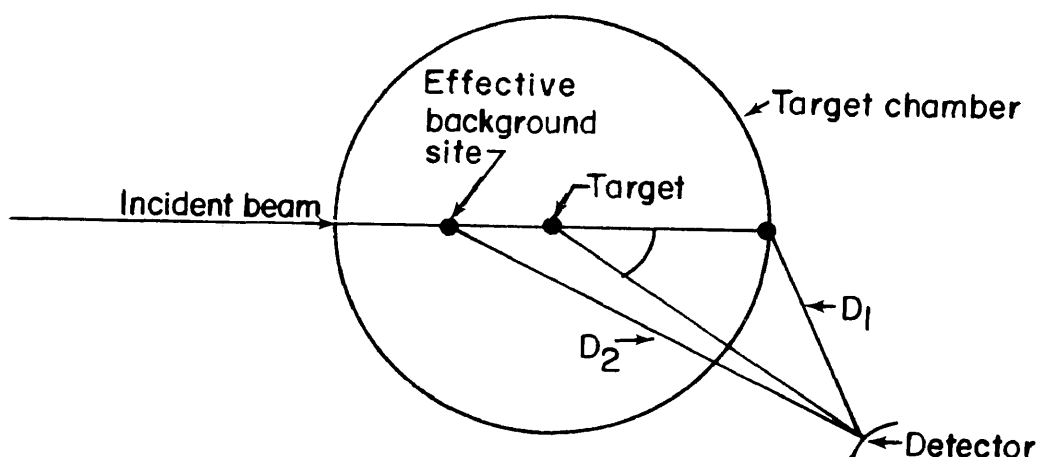
Before making any analysis, certain corrections were made in the experimental data. These corrections were applied to each spectrum measured at the various angles and are explained in detail in this chapter.

First of all, a counting rate correction was applied to the spectra obtained when the target was in place. This correction was necessary because the detector was not counting for the entire time of any given run even though the photons were reaching the detector over the entire time of the run. The correction was made by multiplying the spectrum from any given run by the ratio of the clock time to the live time for that particular run where the clock time is the time required to make the run and the live time is actual counting time.

Corrections to the background spectra were somewhat more involved. There were three basic corrections to these spectra: (a) a geometrical correction, (b) a charge ratio correction, and (c) a counting rate correction. Let C_o be the original background spectrum and let C be the corrected background spectrum. Applying the three corrections listed above, the equation representing C can be written as

$$C = C_o \frac{D_1}{D_2} \frac{Q_2}{Q_1} \frac{\text{clocktime}}{\text{live time}} \quad (2)$$

The first correction shown on the right-hand side of equation (2) is the ratio of $\left(\frac{D_1}{D_2}\right)^2$ where D_1 and D_2 are shown in the schematic below. It was assumed that the effective sight of the background was at a point 2 inches in front of the target and on the incident beam line whereas in the background runs the radiation was produced at the back of the chamber. Therefore in order to move the point of production to the assumed effective site and since the bremsstrahlung is inversely proportional to the square of the distance from source to the detector the spectrum for each run was multiplied by the geometrical ratio $\left(\frac{D_1}{D_2}\right)^2$. This correction was made because one would expect that with the target in place the background is produced by the back-scattered electrons in front of the target.



The charge ratio correction shown in equation (2) was necessary because the background runs were made with a much higher chamber charge than existed in the actual background case and the bremsstrahlung is proportional to the incident electron flux. Here Q_1 is the chamber charge with the target out and Q_2 is the charge on the chamber with the target in place. Finally, a counting rate correction was made as shown in equation (2) to account for the dead counting time.

In the first two corrections described above the assumption has been made that the entire background was produced by back-scattered electrons in the chamber walls.

After making all the corrections mentioned in the previous paragraphs of this chapter, the background spectra were subtracted from the spectra measured with the target in place to obtain what will hereinafter be called the actual spectra.

In order to account for the finite resolution of the detector or the so-called "line broadening" the actual spectra were "stripped" (ref. 10), using standard pulse profiles of known sources such as Cs^{137} , Co^{60} , and Na^{22} . In this experiment the NaI(Tl) crystal scintillator has been used as a spectrometer and it has been shown that the response of a scintillator is not unique. This condition of non-uniqueness is due to uncertainties in the intensity of light produced in the detector, the transmission of the light to the photomultiplier, and the conversion of the light into an electrical pulse by the photomultiplier (ref. 11). The result of this nonuniqueness causes the response to be spread out over a range of pulse heights. By referring

to figure 3 one can see the effects of a nonunique response or the so-called "line broadening." Here the source was of known strength and if an ideal spectrometer had been used one would expect only two points on this curve, one for the 0.51 MeV energy and one for the 1.28 MeV energy. However, it can be seen that instead of two points the spectrum was spread out or broadened and this indicates the inability of the detector to correctly resolve each photon.

Before the process of stripping was performed, the number of counts in the peaks of the calibration source curves, figures 3 and 5, associated with each discrete gamma ray of the given source was determined. This was also necessary because of the finite resolution of the detector and was accomplished by extrapolation of the curves. For instance, the curve shown in figure 3 shows two peaks for Na^{22} (0.51 and 1.28 MeV). The 1.28 peak positioned approximately in channel 380 contributes to the 0.51 MeV peak in channel number 70 and, hence, this contribution must be subtracted from the 0.51 MeV peak. After appropriate adjustments of the curves, the area under each curve and hence the total number of counts associated with the discrete energy peaks were determined. The ratio of peak height in counts to the total counts was then plotted as a function of energy.

The process of stripping was performed in the following manner. The actual spectrum at each angle was divided into strips 50 keV wide. Starting at the high energy end of the spectrum and at the center of each strip, representative pulse profiles of the known sources were plotted in each strip. The representative pulse profiles had a peak

energy as near equal to the mean strip energy as possible. As each profile was drawn in, it was subtracted from the composite spectrum to remove the contribution of that pulse. After completion of this process, the peak height and mean energy are known for each strip. By using the peak to total count ratio as a function of energy, which was plotted earlier, the corrected number of photons at each mean energy could then be counted. In this way the composite spectrum was unfolded and reduced to the so-called stripped spectrum and the nonunique response of the detector was accounted for.

Finally, the stripped spectra were corrected for the absorption in the walls of the target chamber, the absorption in the protective aluminum cover on the NaI(Tl) crystal, and for crystal efficiency. The curve showing the efficiency of the detector as a function of energy is presented in figure 9 and is the same as that in reference 6.

CHAPTER IV

RESULTS AND DISCUSSION

The analysis and results of all the data after application of the corrections shown in the previous chapter are presented in this chapter. In all cases, the results are presented on a per electron basis. The data were reduced to various forms and compared to theoretical calculations which were previously discussed.

Bremsstrahlung Intensity

The primary purpose of the experiment was to measure the bremsstrahlung or photon intensity at the various angles from 15° to 135° . Therefore, the photon intensity is plotted in figure 10 as a function of these angles for several energy ranges. The spectra for the two energy ranges 0.63 MeV to 0.78 MeV and 0.83 MeV to 1.0 MeV have been adjusted so that they have the same value as the 0.38 MeV to 0.58 MeV spectra at 15° . As expected, the photon intensity decreases with an increase in photon energy and angular emission.

Angular Distribution

The photon intensity was further reduced to obtain the total radiated intensity, $I(\theta)$, as a function of emission angle. Here, the total radiated intensity is defined to be the total energy radiated in the small solid angle subtended by the detector to the center of the target and was obtained by multiplying the photon intensity in each

strip by the mean energy of the strip. The angular distribution, $I(\theta)$, for the photon energy range 0.38 MeV to 1.0 MeV is shown in figure 11, and

$$I(\theta) = \sum_{k=0.38}^{1.0} k(N(k))$$

where k is the photon energy and $N(k)$ is the number of photons of energy k . Also shown in figure 11 are the calculations of $I(\theta)$ based on the theoretical model. It can be seen that the experimental and theoretical calculations are in reasonable agreement. They are always within a factor of 1.5 of each other, and the theoretical is always less than the experimental except at the photon emission angle of 15° .

A fifth-order polynomial has been fitted to the experimental curve for $I(\theta)$ in terms of Legendre polynomials. This expression is

$$I(\theta) = a_0 + a_1 P_1(\cos \theta) + a_2 P_2(\cos \theta) + a_3 P_3(\cos \theta) + a_4 P_4(\cos \theta)$$

where

$$\begin{aligned} a_0 &= 1.60 \times 10^{-7} & a_2 &= 6.80 \times 10^{-8} & a_4 &= 1.01 \times 10^{-8} \\ a_1 &= 1.41 \times 10^{-7} & a_3 &= 7.35 \times 10^{-8} \end{aligned}$$

were obtained from the fit.

Efficiency of Production

One of the more important parameters that was calculated is the efficiency of the bremsstrahlung production where the efficiency is defined as

$$\psi = \frac{\text{Total radiated energy}}{\text{Total incident energy}}$$

In order to obtain the total radiated energy, it was necessary to integrate $I(\theta)$ over 4π steradians, that is

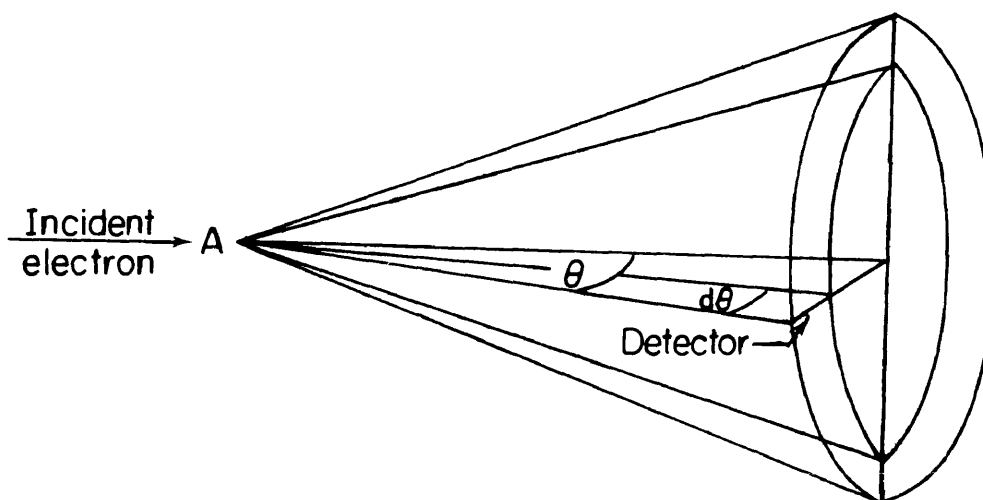
$$I = \int I(\theta) d\Omega$$

where $d\Omega$ is the element of solid angle subtended by the detector to the target. The total incident energy per electron, of course, was 1 MeV. It was found that over the photon energy range of 0.38 MeV to 1 MeV, the experimental efficiency was 0.54 percent compared with the theoretical calculation, as discussed in Chapter I, of 0.52 percent. Thus, the experimental efficiency results are in very good agreement with the theory.

Differential Cross Section

The experimental data were further reduced to obtain the differential cross section $d\sigma/dk d\theta$ which is differential in energy and angle. In order to obtain this parameter, the photon intensity for each strip at each angle was divided by the product $\Delta k \Delta\Omega$ where these

two parameters have been previously defined. This put the data on a per MeV-steradian basis. The data were then multiplied by the total number of steradians contained in the solid angle subtended by the annulus shown in the schematic below, and divided by $d\theta$ resulting in the cross section $d\sigma/dk d\theta$.



This cross section has units of $\text{cm}^2/\text{electron-MeV-radian}$. A comparison of the experimental cross sections with the theoretical Born approximation cross sections is shown in figure 12 for all angles at which the spectra were accumulated. The experimental results are in good agreement with the theoretical results, especially in the region of about 0.45 MeV to 0.9 MeV. The cross section decreases as the energy increases, as one would expect. One would also expect the cross section to peak in the forward direction, that is, to increase as the angle θ decreases. Figure 13 is presented to show that, indeed, the experimental cross section behaves in this manner.

Another differential cross section of importance is $d\sigma/dk$, which is differential with respect to energy only and is referred to as the total differential cross section. This cross section was obtained by integrating $d\sigma/dk d\theta$ over all angles, and is shown in figure 14 where a comparison is made with the calculations discussed in Chapter I. Again, it can be seen that the experimental results are in good agreement with the theoretical results. One can also see the expected decrease in the cross section as the photon energy increases.

In general, the experimental results presented in this chapter are in reasonable agreement with the theoretical model discussed in Chapter I and the trends in the data behave as expected.

CHAPTER V

CONCLUDING REMARKS

In general, the experimental results presented in this paper were as expected. For example, the photon or bremsstrahlung intensity peaked in the forward direction and increased as the photon energy decreased. The angular distribution of the total radiated intensity agreed reasonably well with the theoretical calculations based on equation (1), Chapter I, always within a factor of 1.5. With the exception of the 15° emission angle the experimental values were larger than the theoretical values at all angles and changed most rapidly in the interval from 0° to 60° . Calculations of the bremsstrahlung production efficiency over the energy range from 0.38 MeV to 1 MeV agreed within 4 percent with the theoretical model even though no complete thick target bremsstrahlung theories are available. Experimental values of the cross sections $d\sigma/dk d\theta$ and $d\sigma/dk$ were found to be in reasonable agreement with the theoretical results, especially in the energy range from 0.45 MeV to 0.9 MeV. A slight depression or concave deflection was noted in the experimental curves at all angles. It is not known whether this is real or due to experimental error. However, thick target bremsstrahlung is complicated by electron back-scattering and absorption in the target. Similar depressions were noted in the experimental data presented in reference 12.

REFERENCES

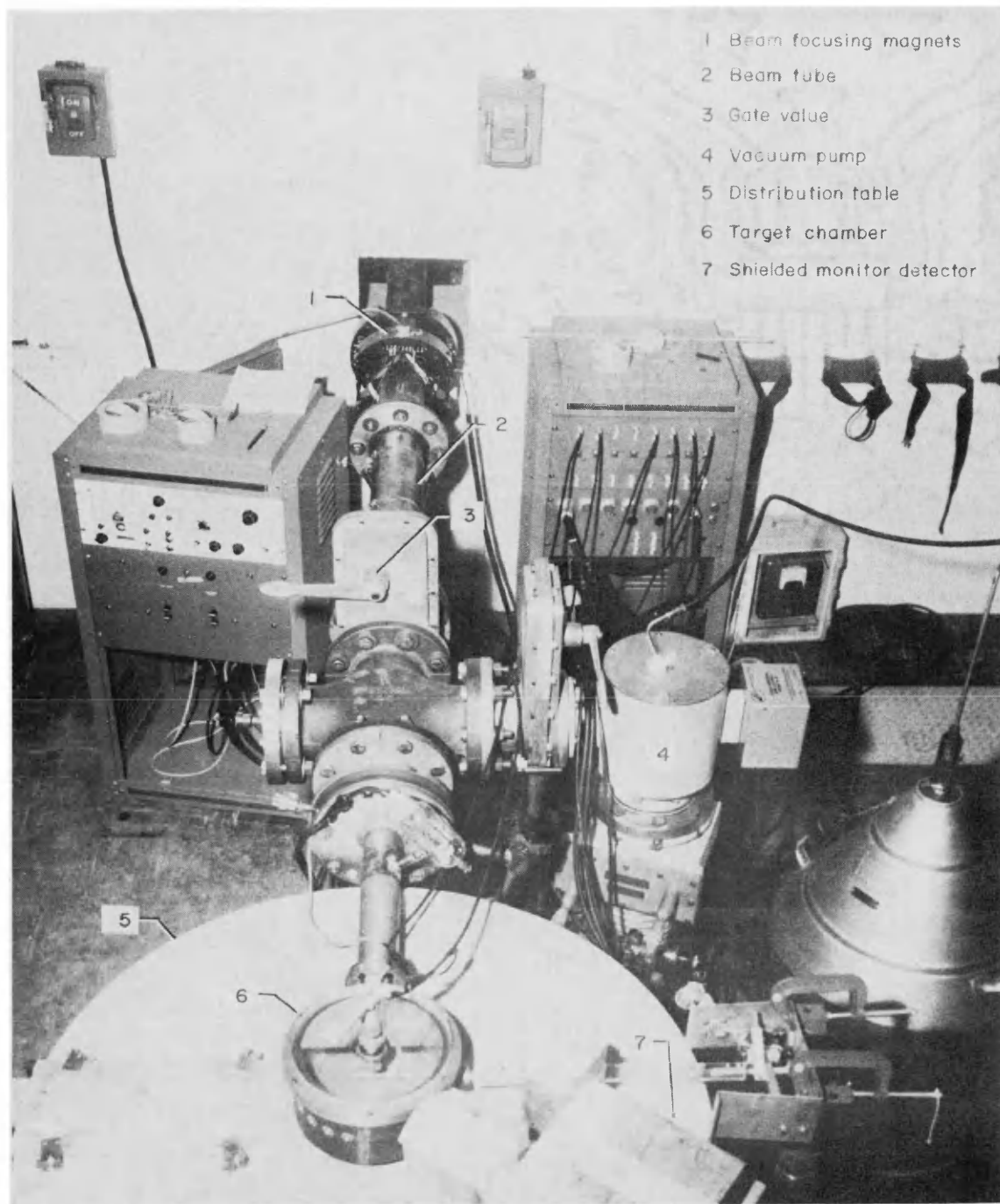
1. Foelsche, Trutz: Estimates of Radiation Doses in Space on the Basis of Current Data. Third International Space Science Symposium, Washington, D.C., April 30 - May 9, 1962. Reprinted from: Life Sciences and Space Research, edited by R. B. Livingston, A. A. Imshenetsky, G. A. Derbyshire.
2. Koch, H. W.; and Motz, J. W.: Bremsstrahlung Cross-Section Formulas and Related Data. Reviews of Modern Physics, 31, no. 4, 920, October 1959.
3. Segre, E.: Experimental Nuclear Physics. 1, John Wiley and Sons, New York, 1960.
4. Bethe, H. A.; and Heitler, W.: Proceedings of the Royal Society (London), A146, 83, 1934.
5. Rossi, Bruno: High Energy Particles. Prentice-Hall, Inc., Englewood Cliffs, N.J., 1961.
6. Ferguson, D. N.: Bremsstrahlung Production in Lanthanum Thick Targets. Thesis presented to Faculty of the Department of Physics, College of William and Mary, Williamsburg, Virginia, November 1965.
7. Goudsmit, S.; and Saunderson, J. L.: Multiple Scattering of Electrons. Physical Review, 57, 24, 1939.
8. Berger, Martin J.: Monte Carlo Calculations of the Penetration and Diffusion of Fast Charged Particles. Chapter V of Methods in Computational Physics, 1. Edited by Berni Alder, Sidney Fernback, and Manuel Rotenberg. Academic Press, New York, 1963.
9. Evans, R. D.: The Atomic Nucleus. McGraw-Hill Book Company, Inc., New York, 1955.
10. Singh, Jag J.; Adams, Richard; Gross, Chris: X-Ray Spectra Produced When Thick Silicon Targets are Bombarded With 1.05 and 1.25 Million Volts Electrons. NASA TN D-2773, December 1966.
11. Birks, J. B.: The Theory and Practice of Scintillation Counting. The Macmillan Company, New York, 1964.
12. LTV Research Center: Investigation of Bremsstrahlung Produced by the Interaction of Electrons With Matter. Report No. O-71000/4R-14, June 1964. Contract No. NASw-647.

VITA

Harold Randolph Compton

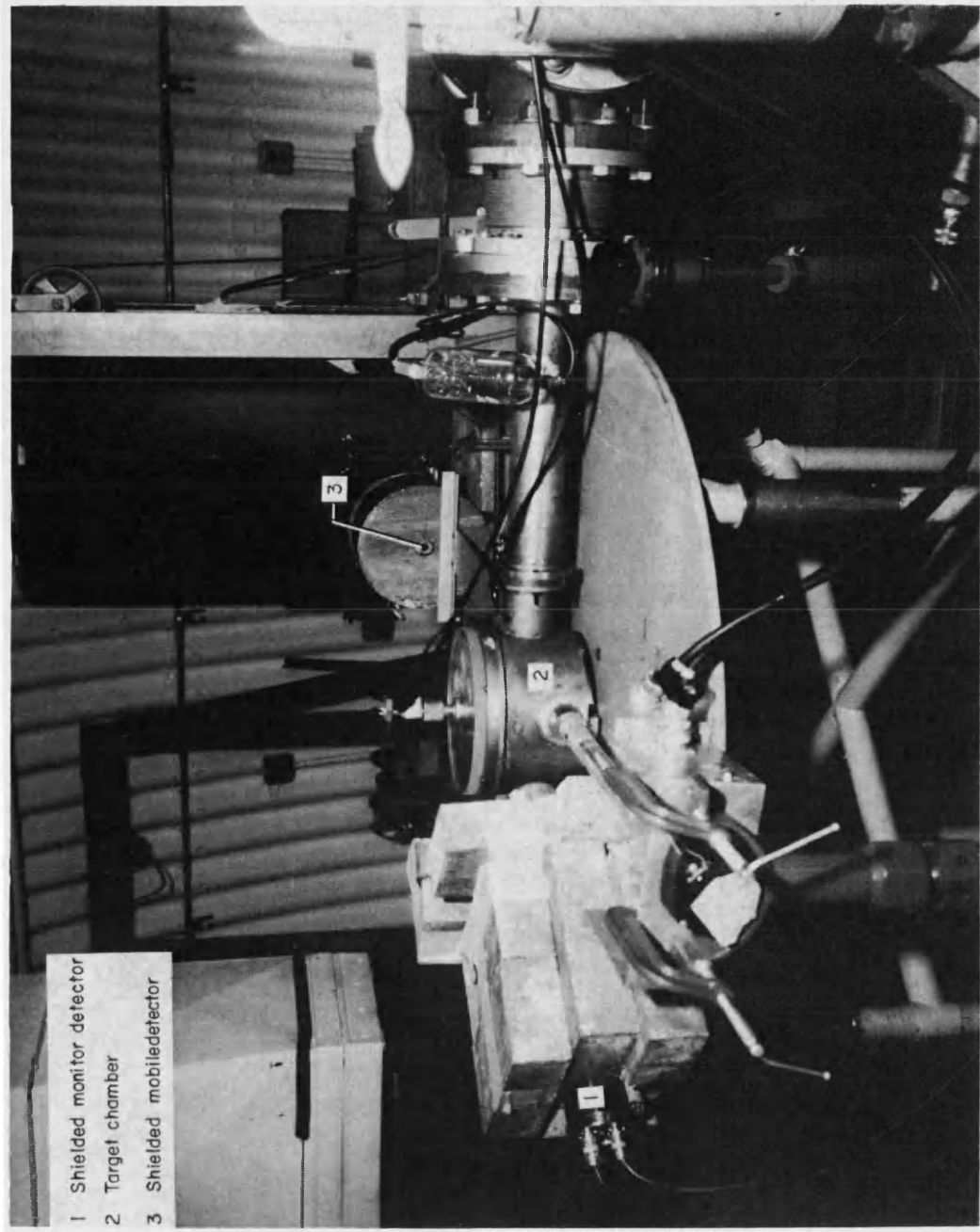
Born in Lynchburg, Virginia, August 14, 1932. Graduated from E. C. Glass High School in Lynchburg, Virginia, June 1950. Served in the United States Army from February 1953 to January 1955. Graduated cum laude with Bachelor of Science in Physics and Mathematics from Lynchburg College, Lynchburg, Virginia, in June 1959. Member of Chi Beta Phi, scientific fraternity, and the National Honor Society. Employed by National Aeronautics and Space Administration, Langley Research Center, Langley Station, Hampton, Virginia, in February 1959.

In 1960 the author enrolled at the College of William and Mary as a graduate student in Physics.



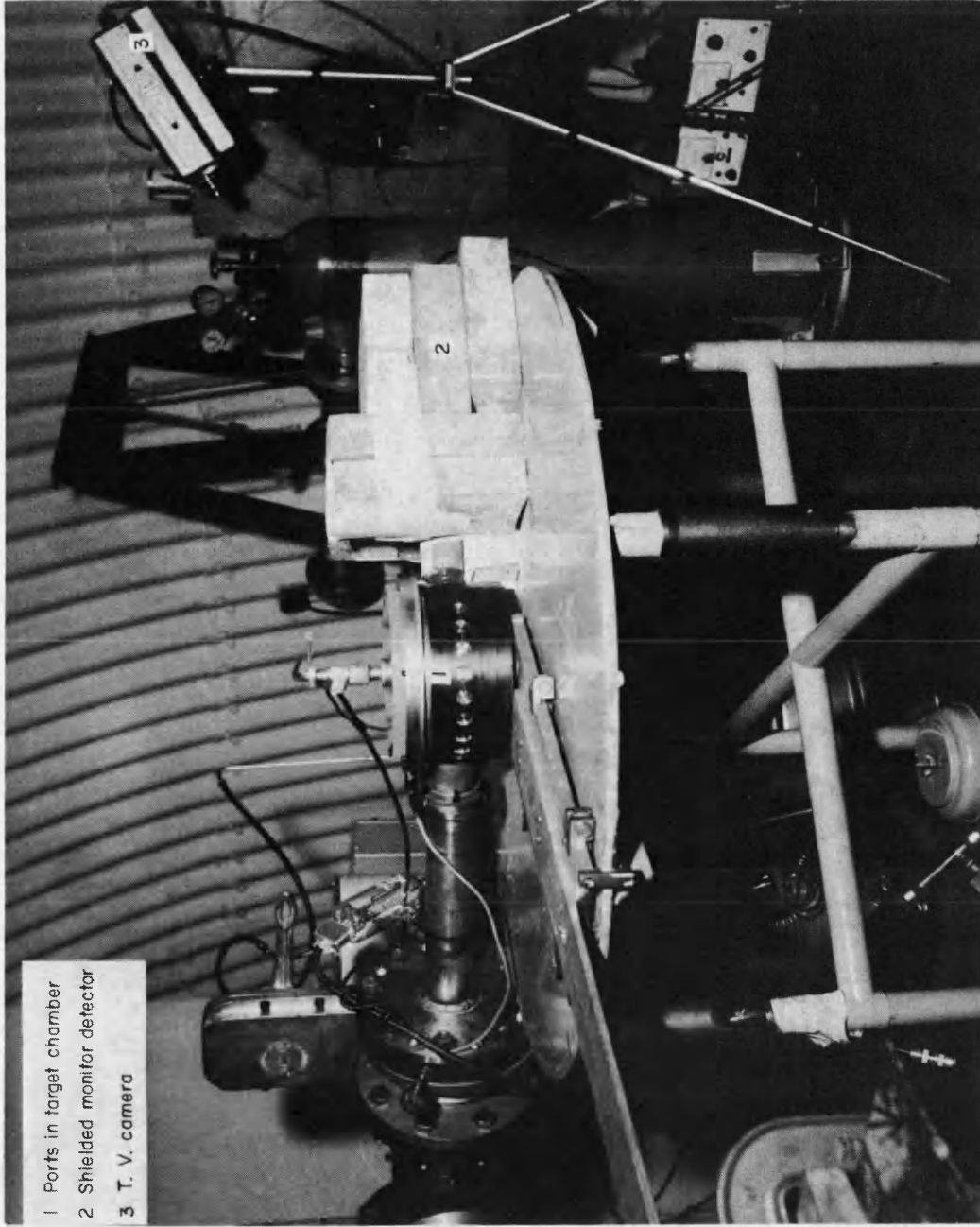
(a) View from above.

Figure 1.- Arrangement of experimental equipment.



(b) View from right side.

Figure 1.- Continued.



(c) View from left side.

Figure 1.- Concluded.

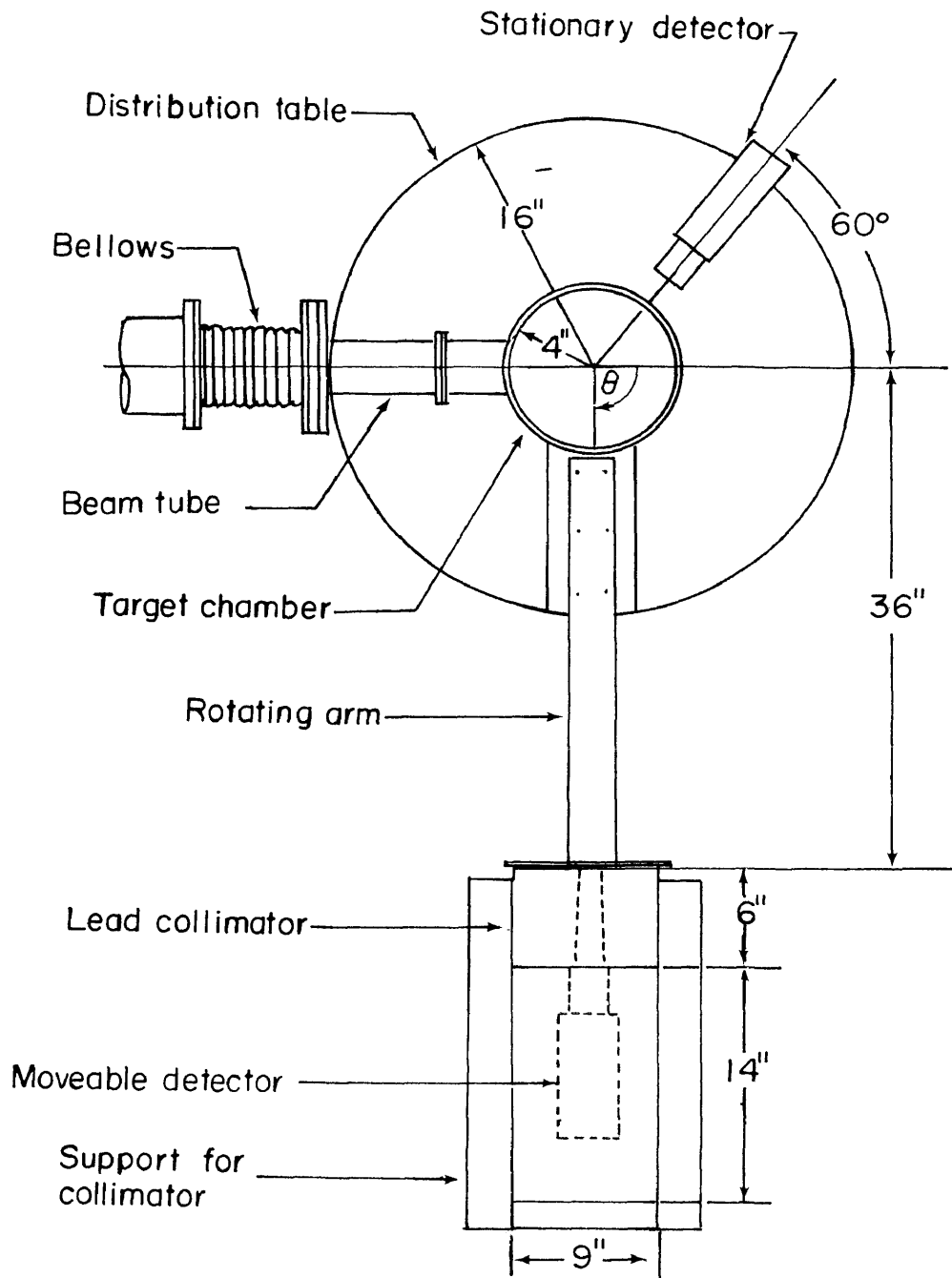


Figure 2.- Schematic of detection arrangement. The angle θ is measured from the forward direction of the incident electron beam to the target-detector line with 0° being in the forward direction.

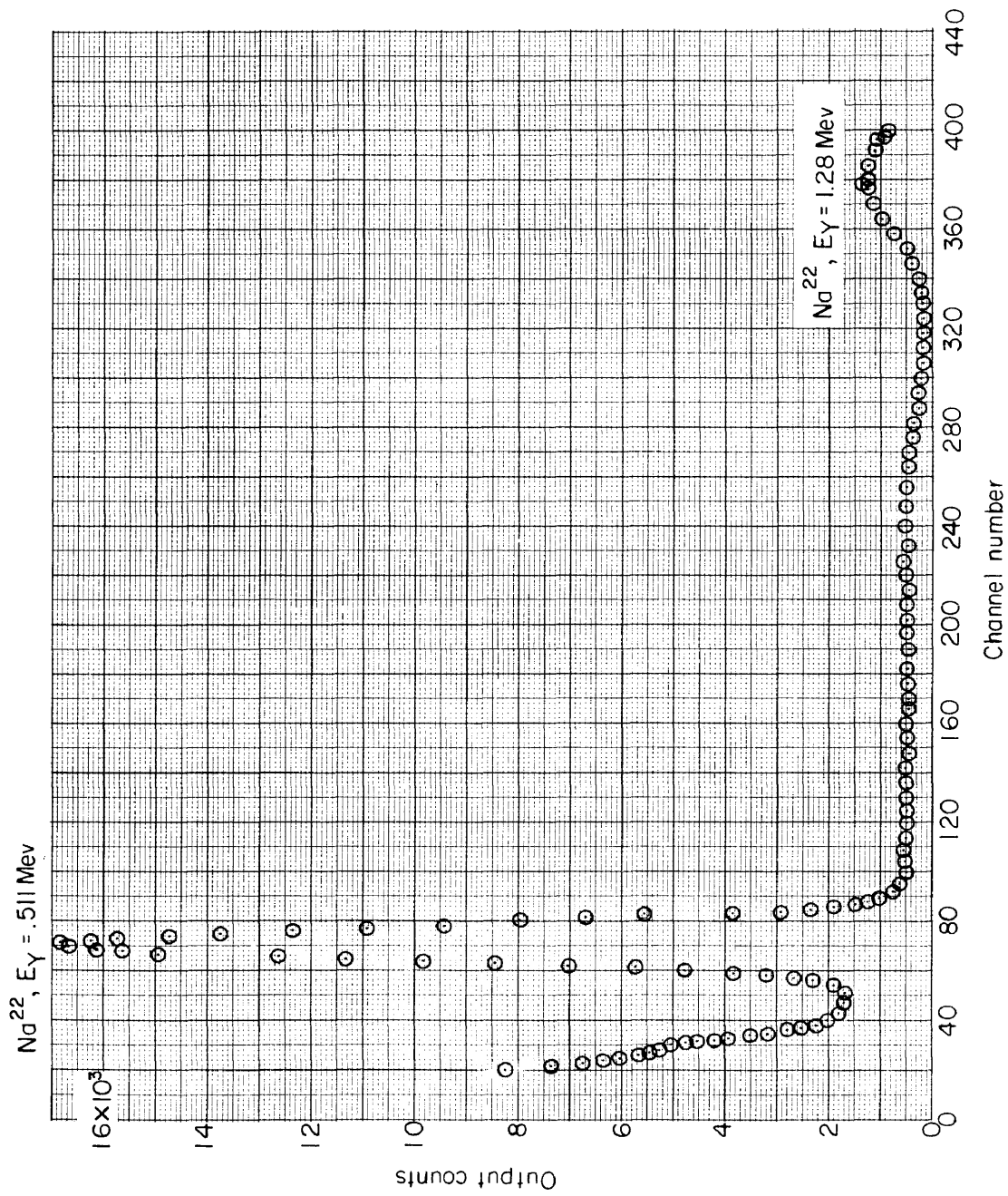


Figure 3.-- Typical spectrum from calibration source Na²² (0.511 MeV and 1.28 MeV).

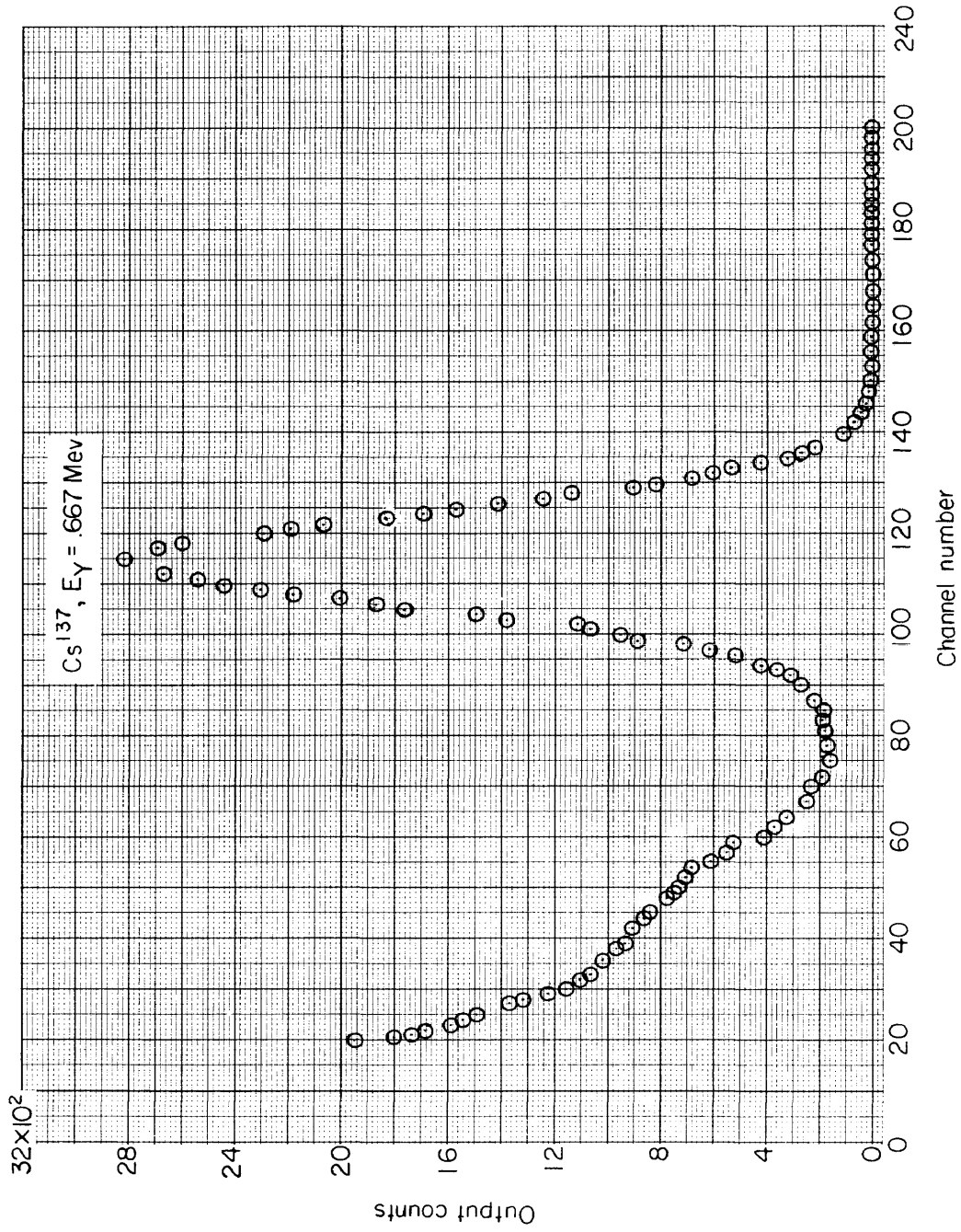


Figure 4.- Typical spectrum from calibration source Cs¹³⁷ (0.667 MeV).

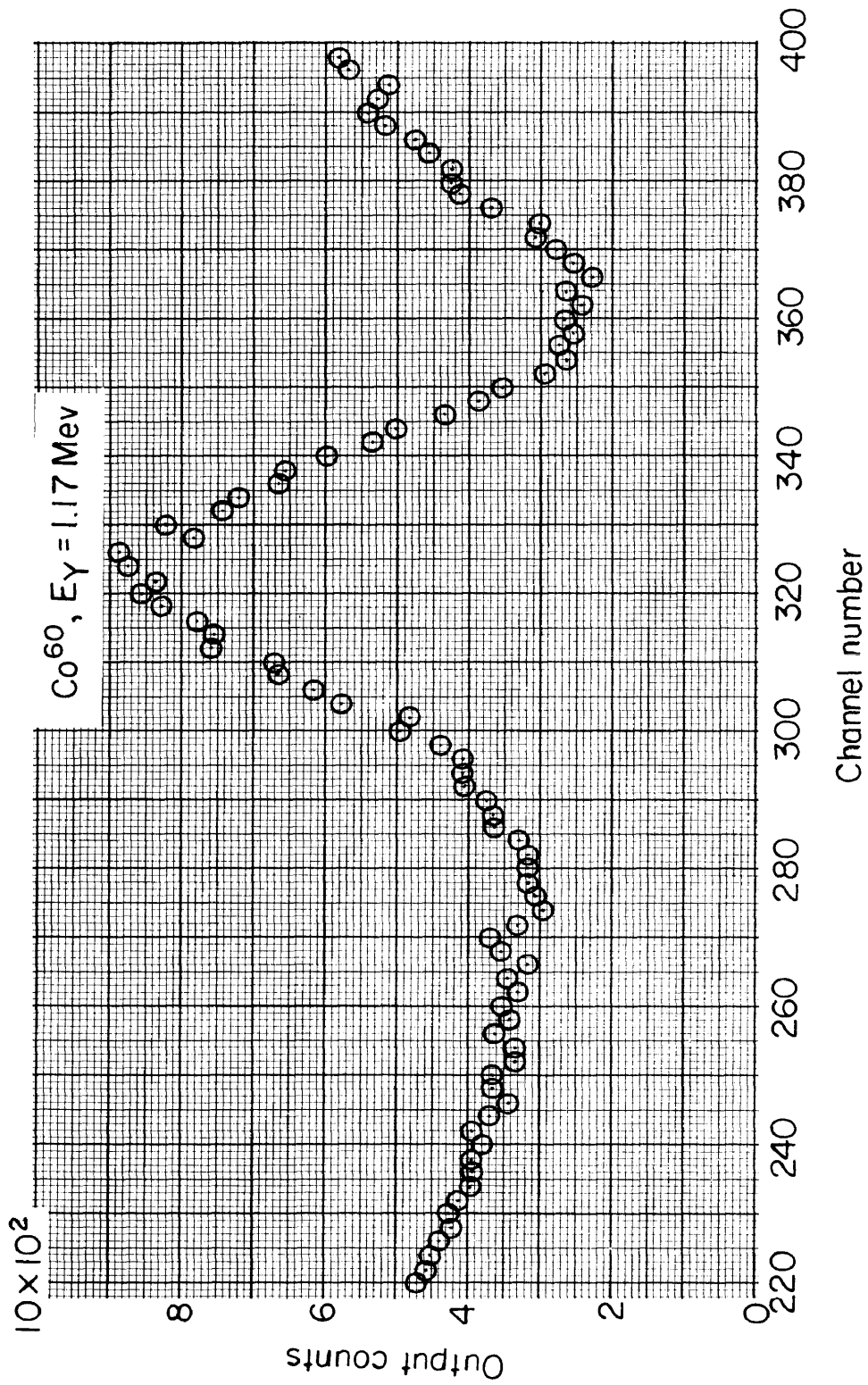


Figure 5.- Typical spectrum from calibration source Co⁶⁰ (1.17 MeV and 1.33 MeV).

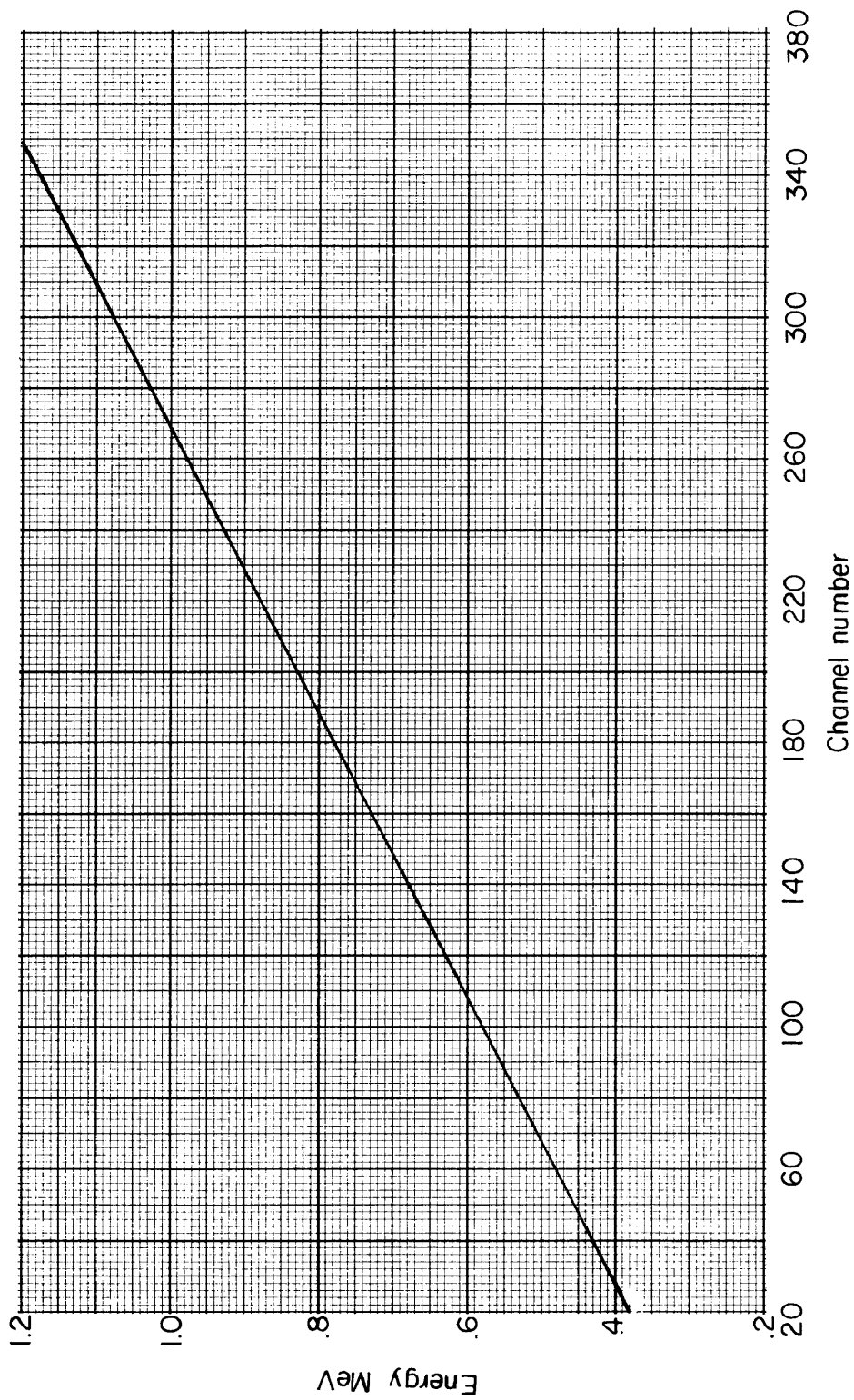


Figure 6.- Typical pulse height analyzer calibration curve.

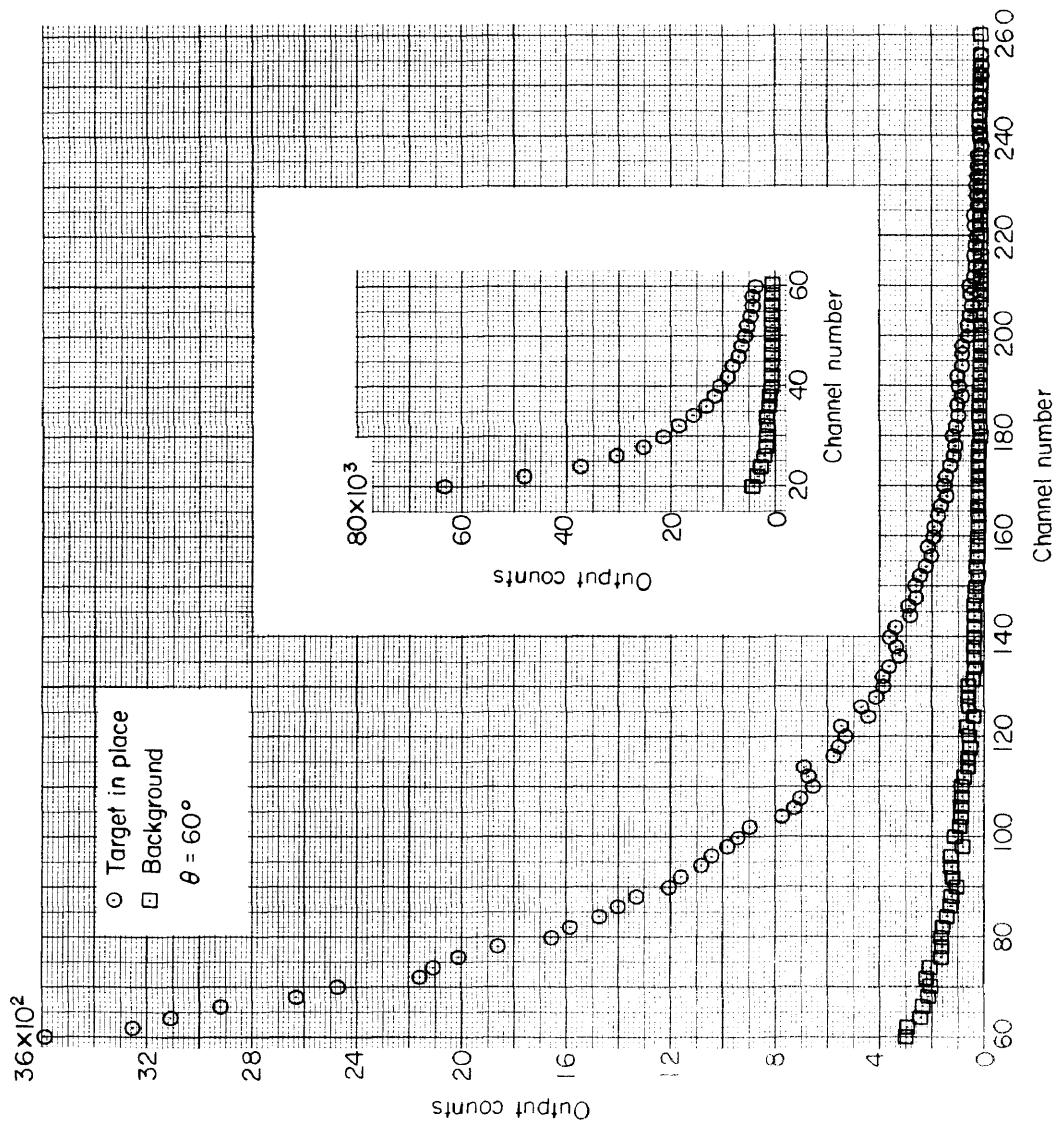


Figure 7.- Typical bremsstrahlung spectrum in the photon energy range 0.38 MeV to 1.0 MeV before any corrections ($\theta = 60^\circ$). Incident electron energy $E_0 = 1.0$ MeV.

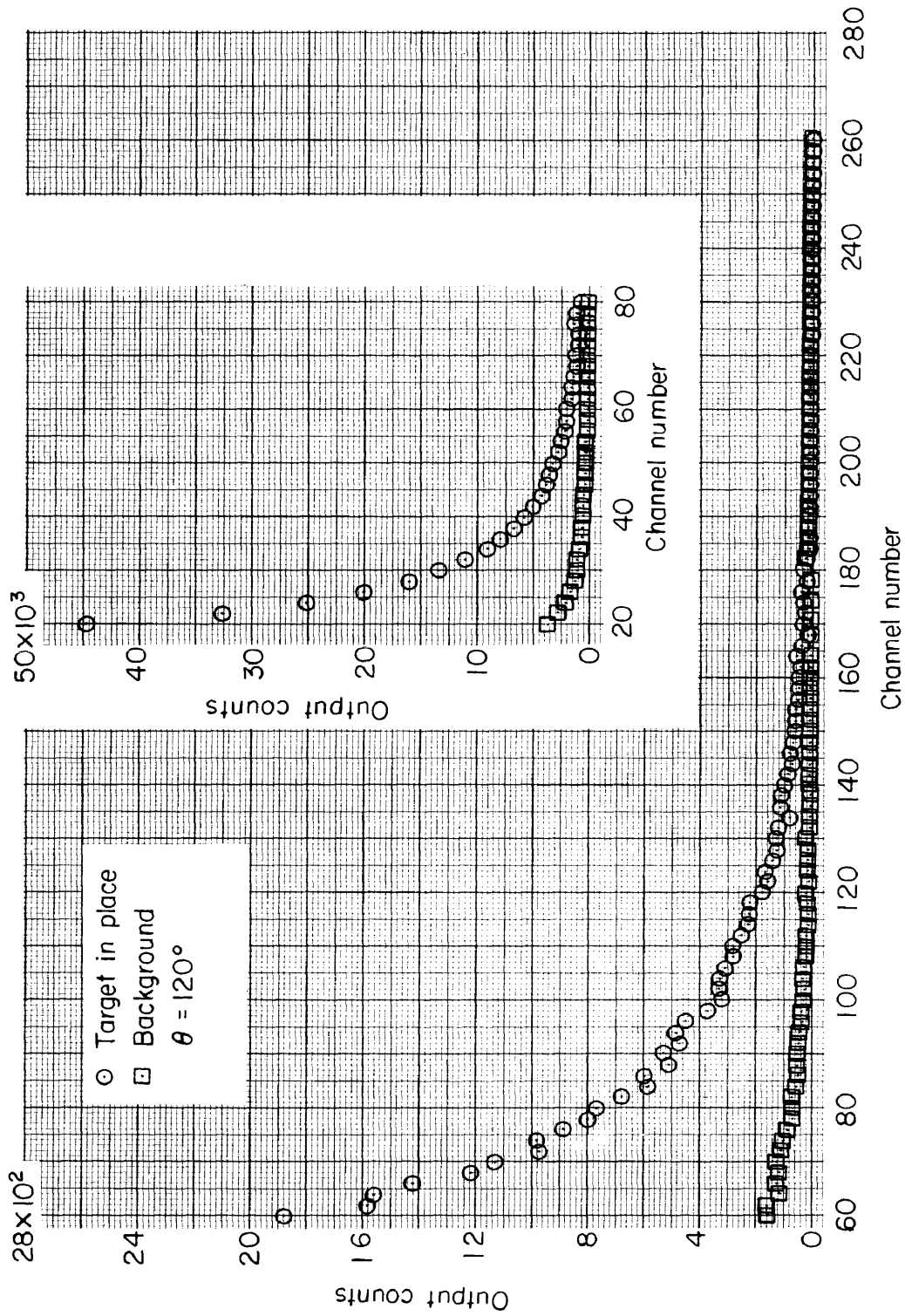


Figure 8.- Typical bremsstrahlung spectrum in the photon energy range 0.38 MeV to 1.0 MeV before any corrections ($\theta = 120^\circ$). Incident electron energy $E_0 = 1.0$ MeV.

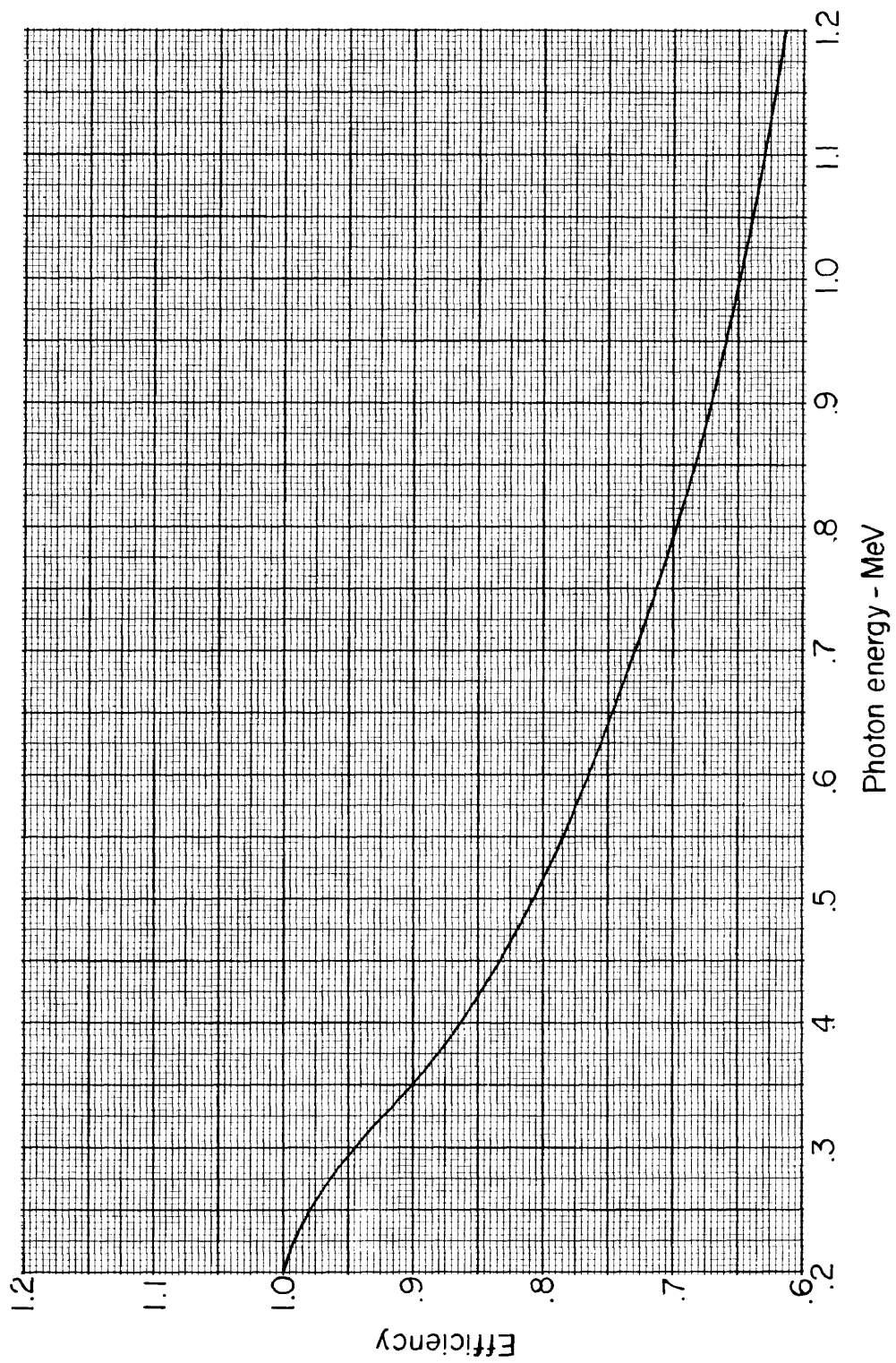


Figure 9.- Detector efficiency.

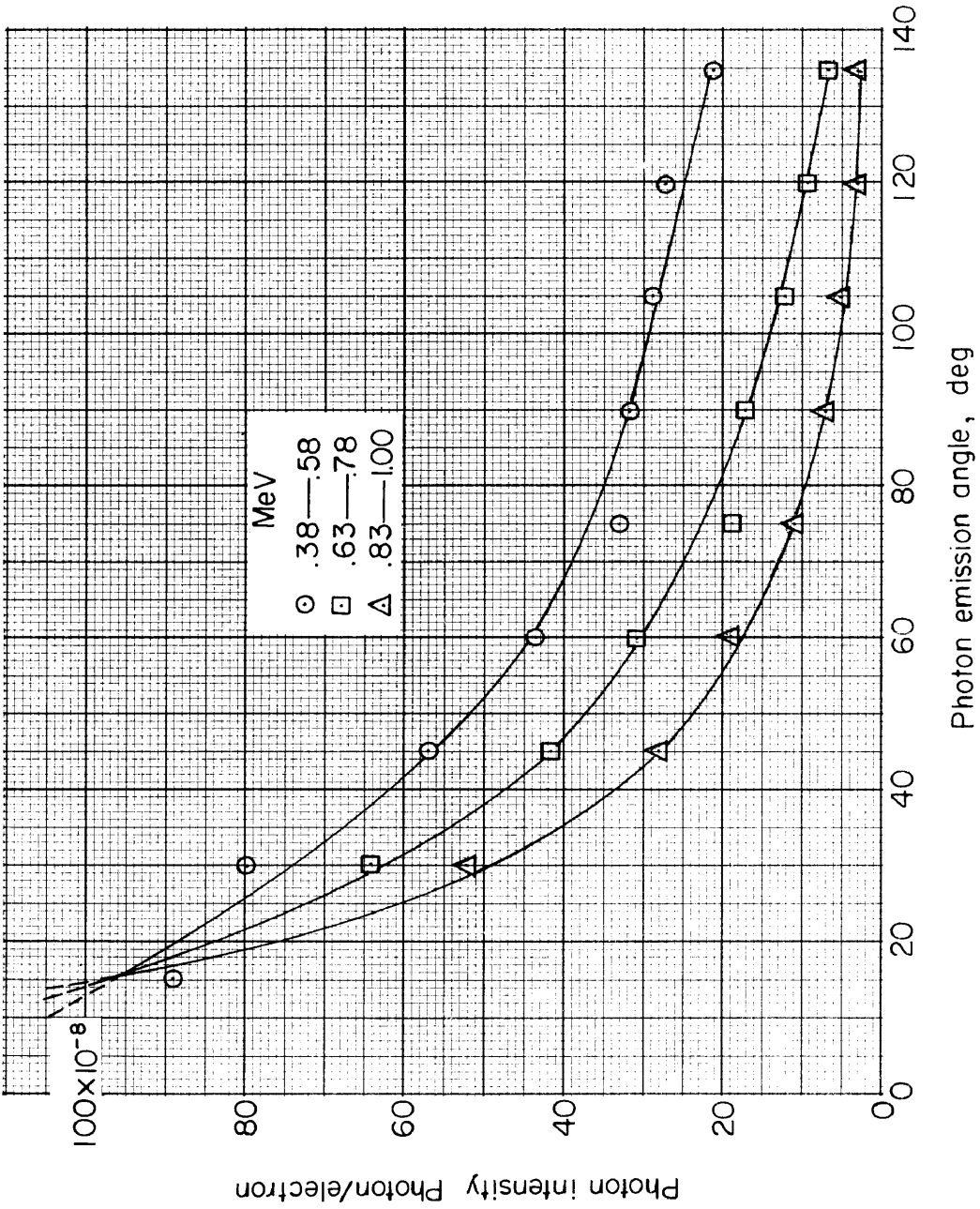


Figure 10.- Photon or bremsstrahlung intensity for several energy ranges. The curves for the energy ranges 0.63 MeV to 0.78 MeV and 0.83 MeV to 1.0 MeV have been adjusted so that they have the same values as that for 0.38 MeV to 0.58 MeV at $\theta = 15^\circ$. Incident electron energy $E_0 = 1.0$ MeV.

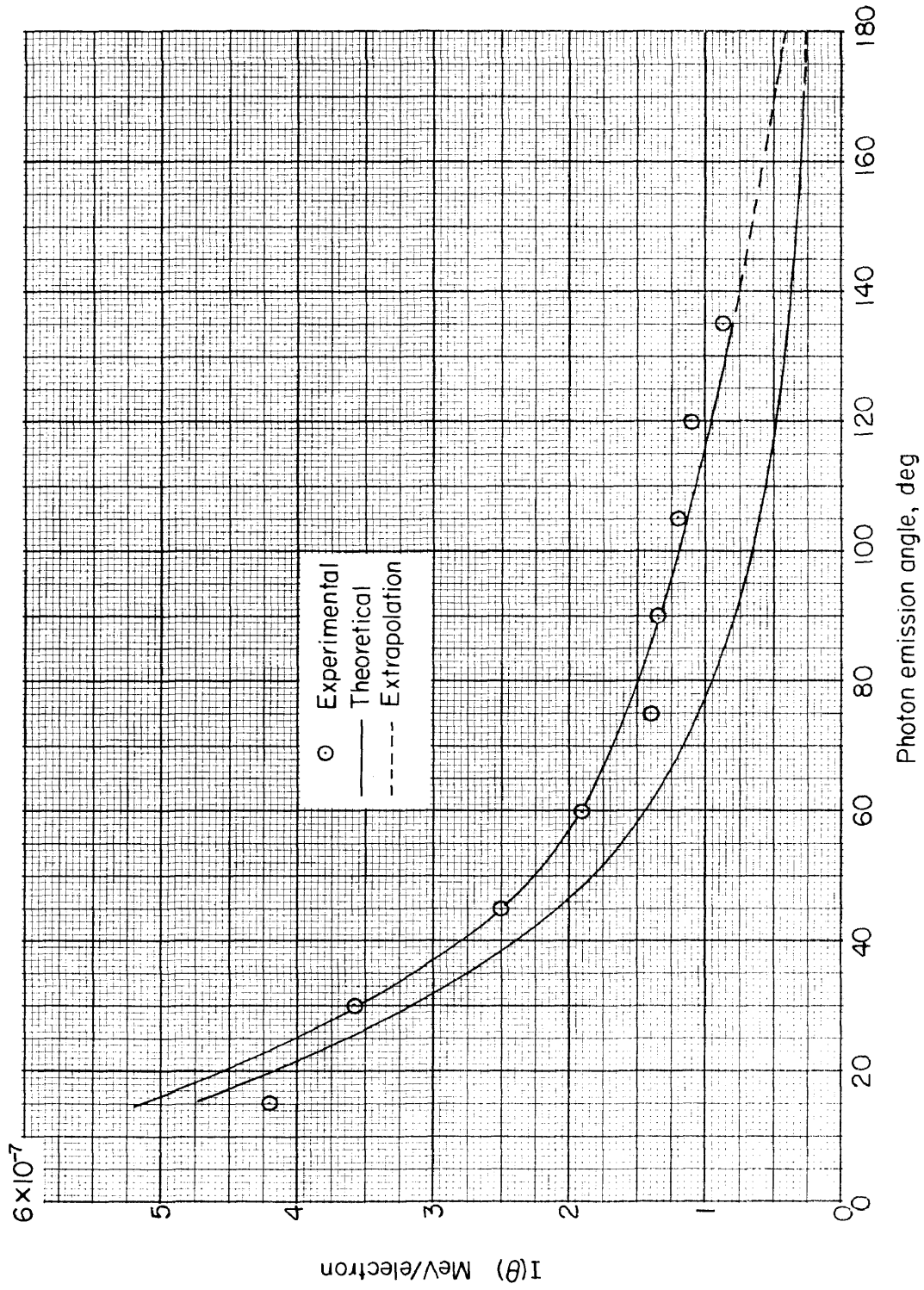


Figure 11.- Angular distribution of total radiated intensity $I(\theta)$ for photon energy range from 0.38 MeV to 1.0 MeV. Incident electron energy $E_0 = 1.0$ MeV.

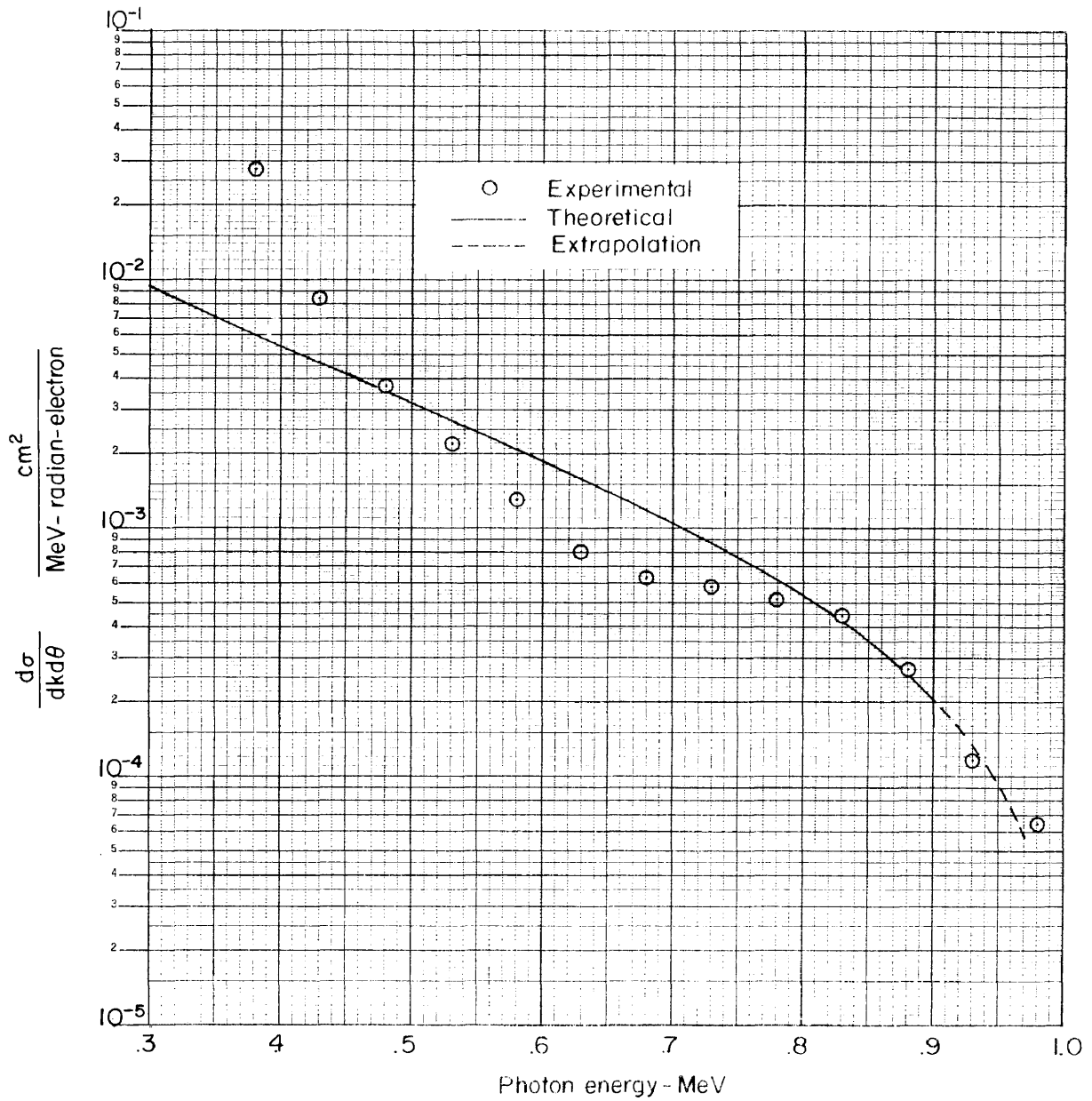
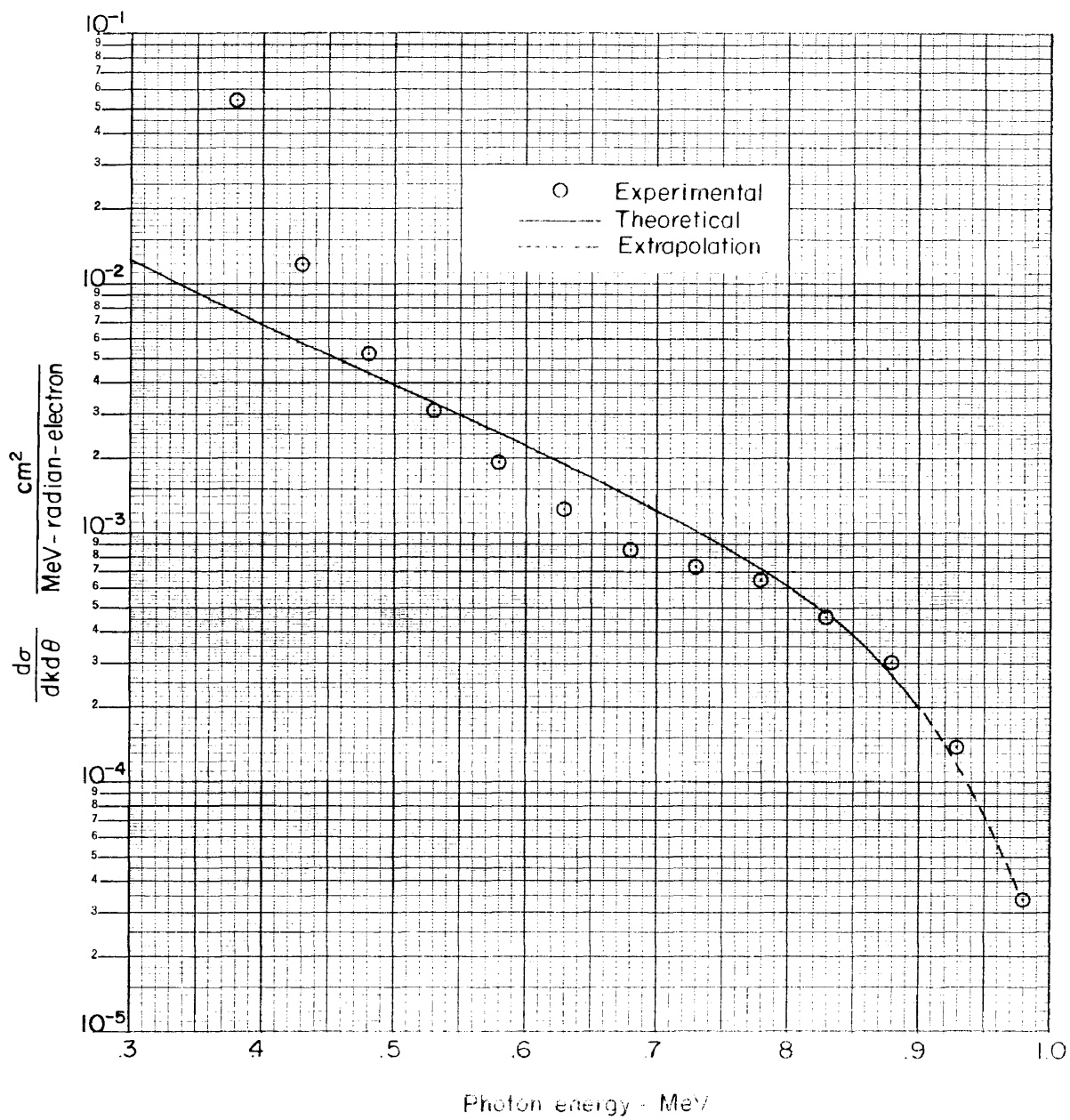
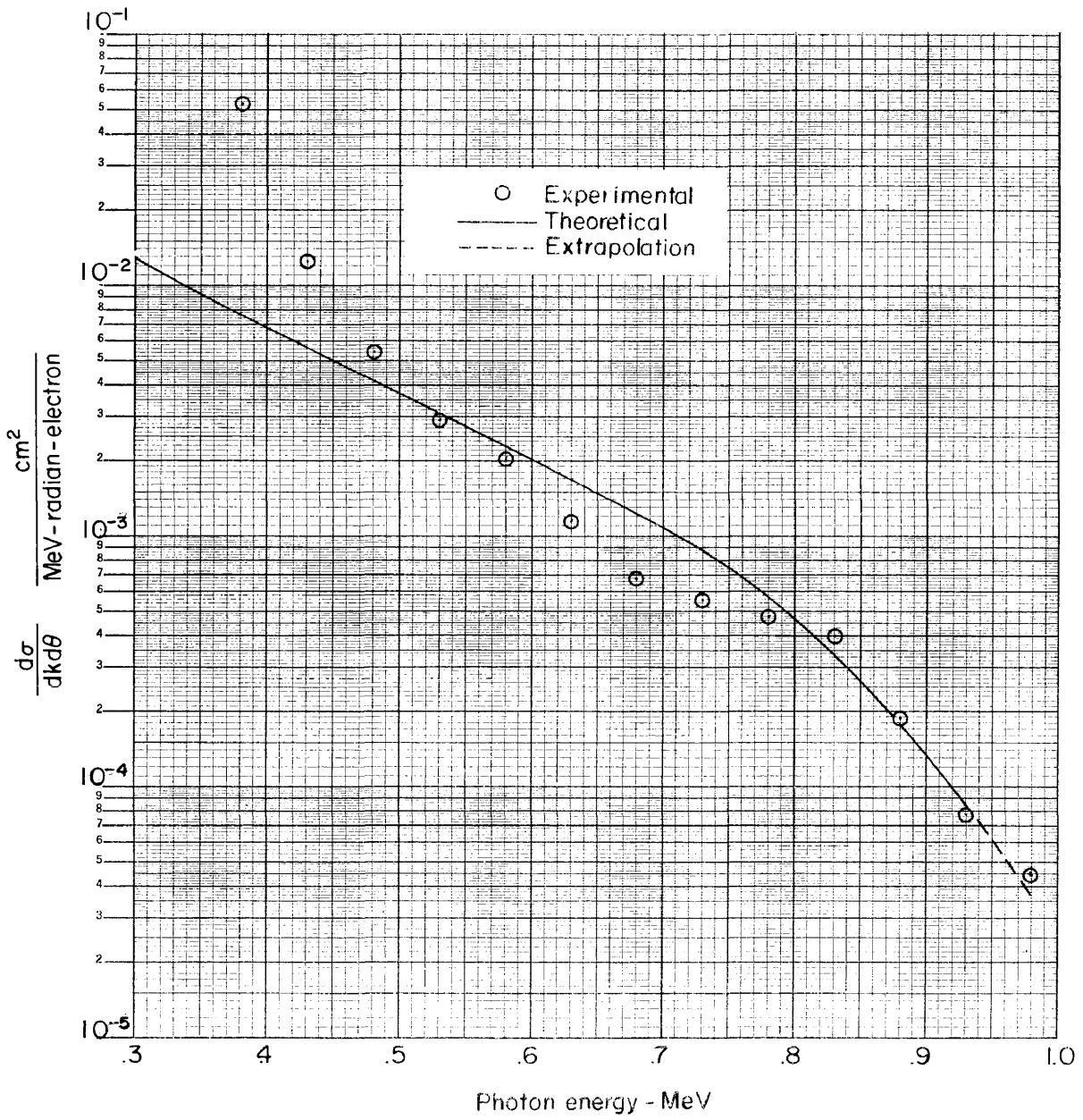
(a) $\theta = 15^\circ$.

Figure 12.- Comparison of experimental bremsstrahlung differential cross section $\frac{d\sigma}{dk d\theta}$ with the Born-approximation cross section. Incident electron energy $E_0 = 1.0$ MeV.



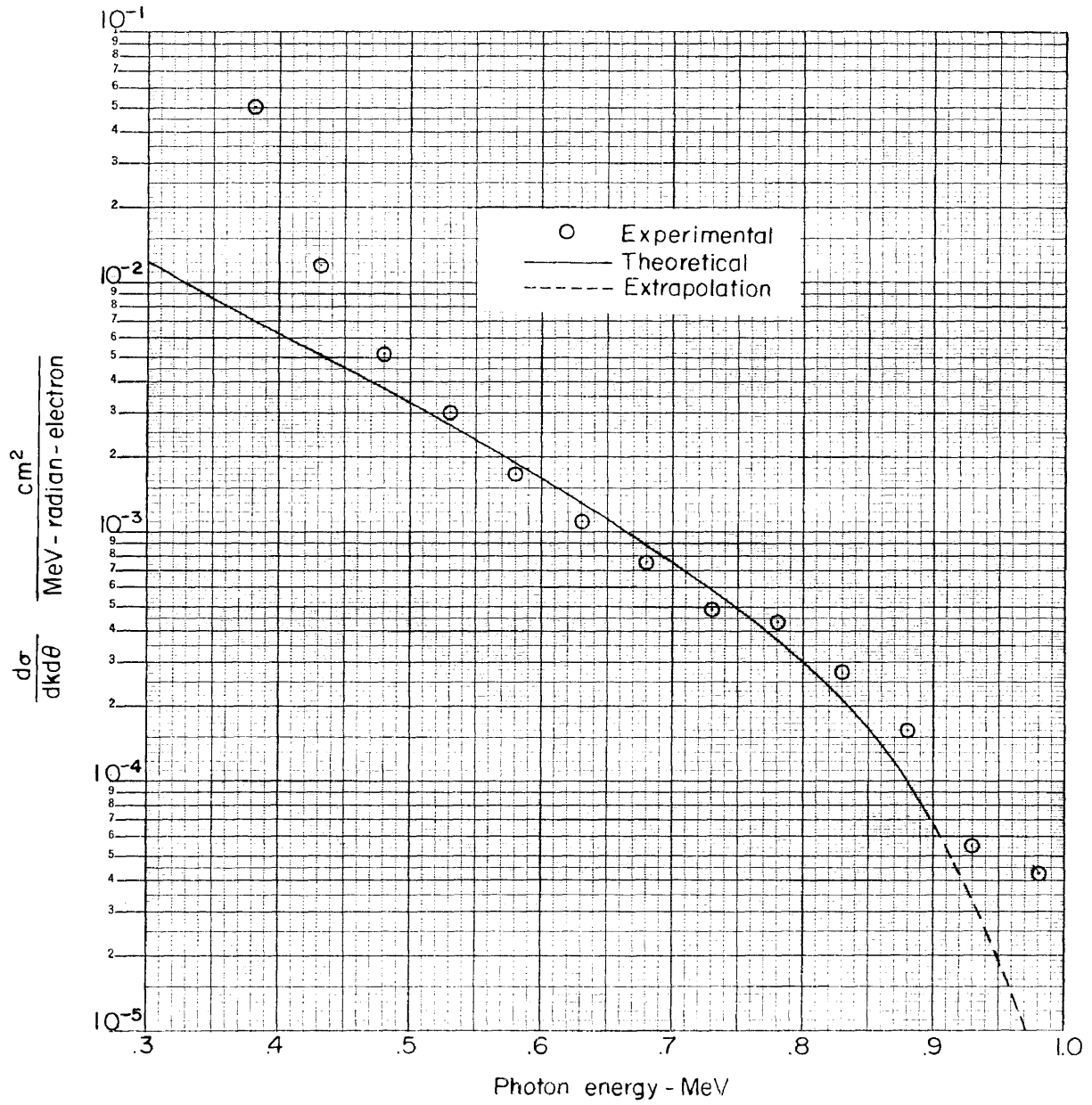
(b) $\theta = 30^\circ$.

Figure 12.- Continued.



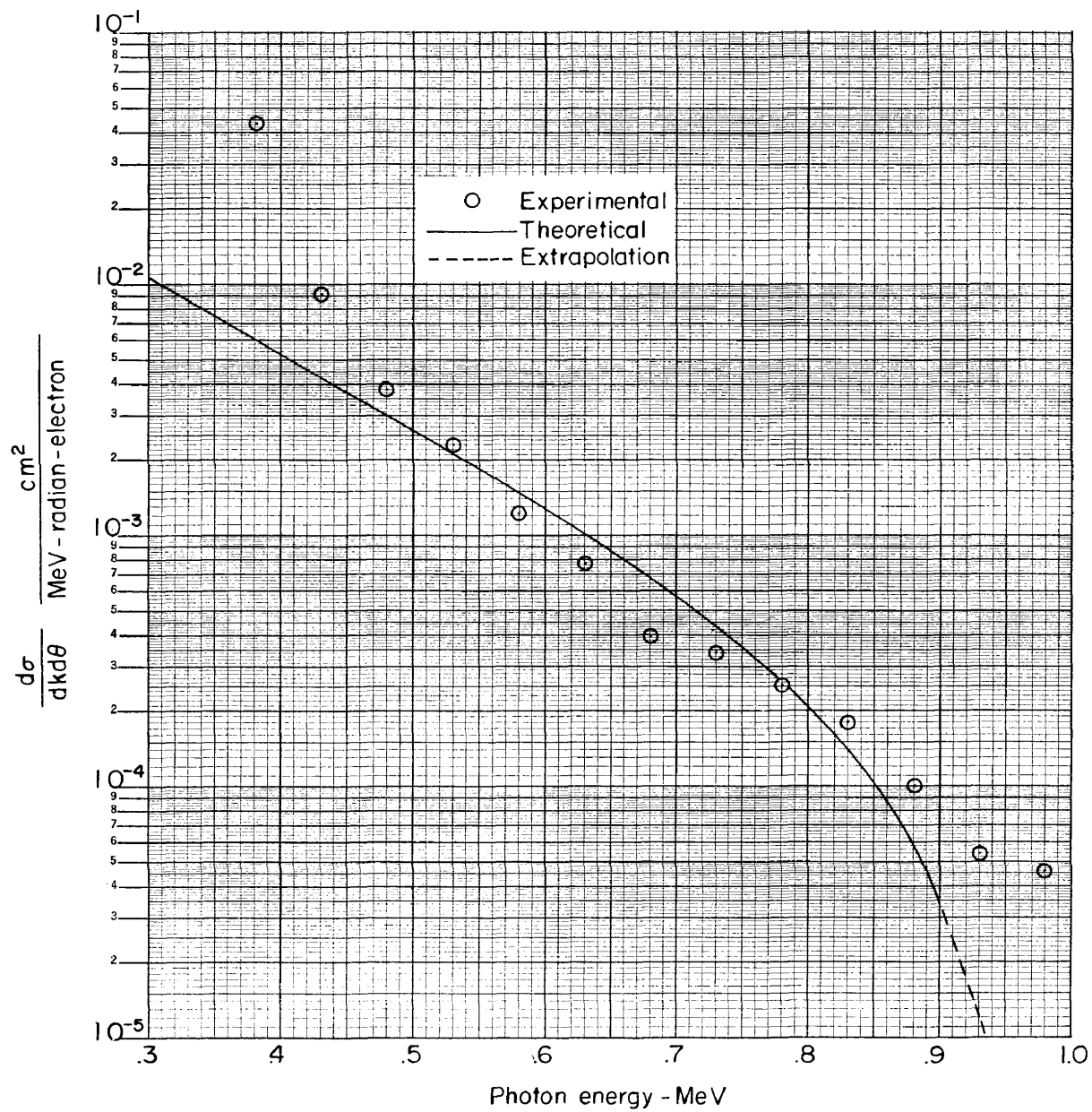
(c) $\theta = 45^\circ$.

Figure 12.- Continued.



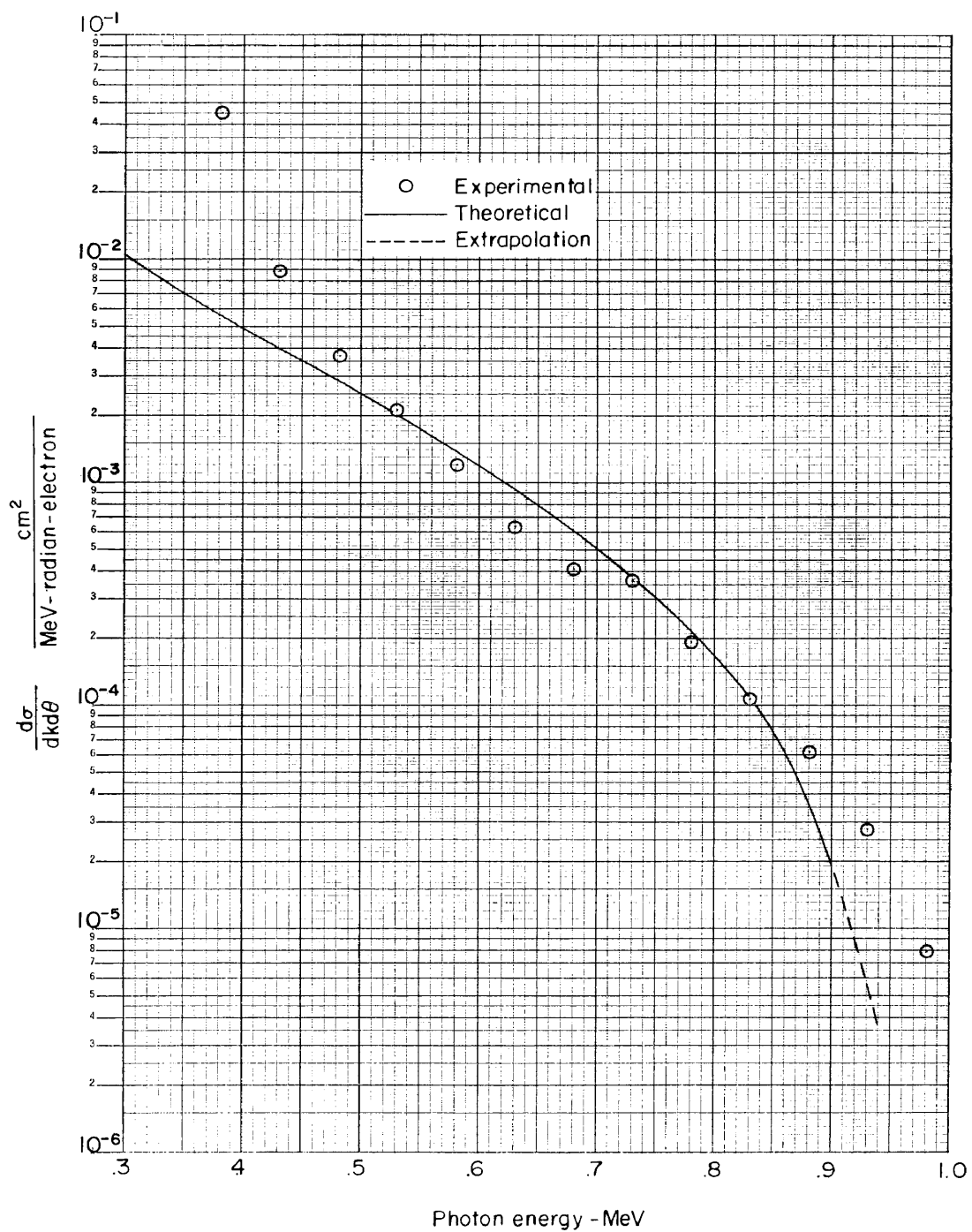
(d) $\theta = 60^\circ$.

Figure 12.- Continued.



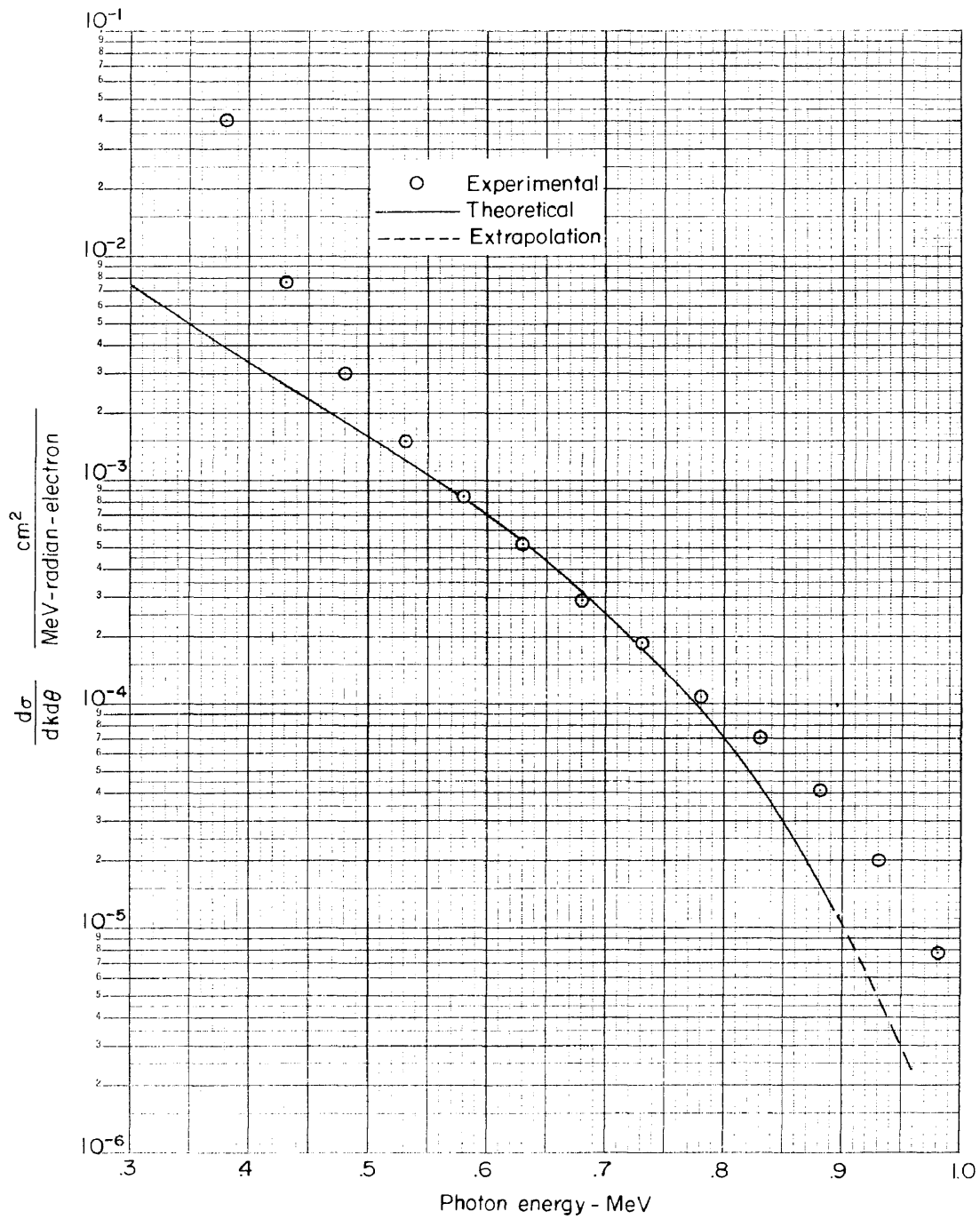
(e) $\theta = 75^\circ$.

Figure 12.- Continued.



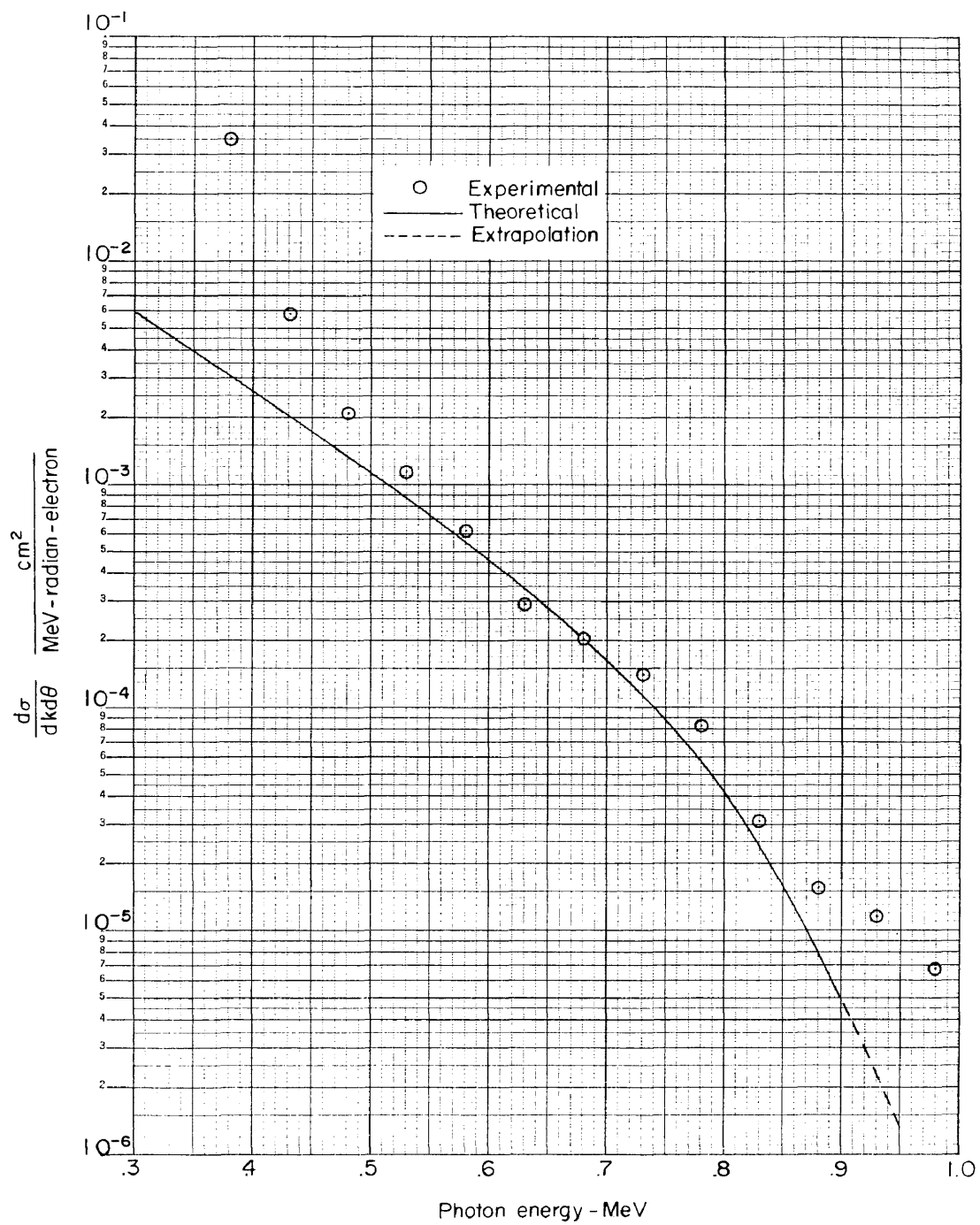
(f) $\theta = 90^\circ$.

Figure 12.- Continued.



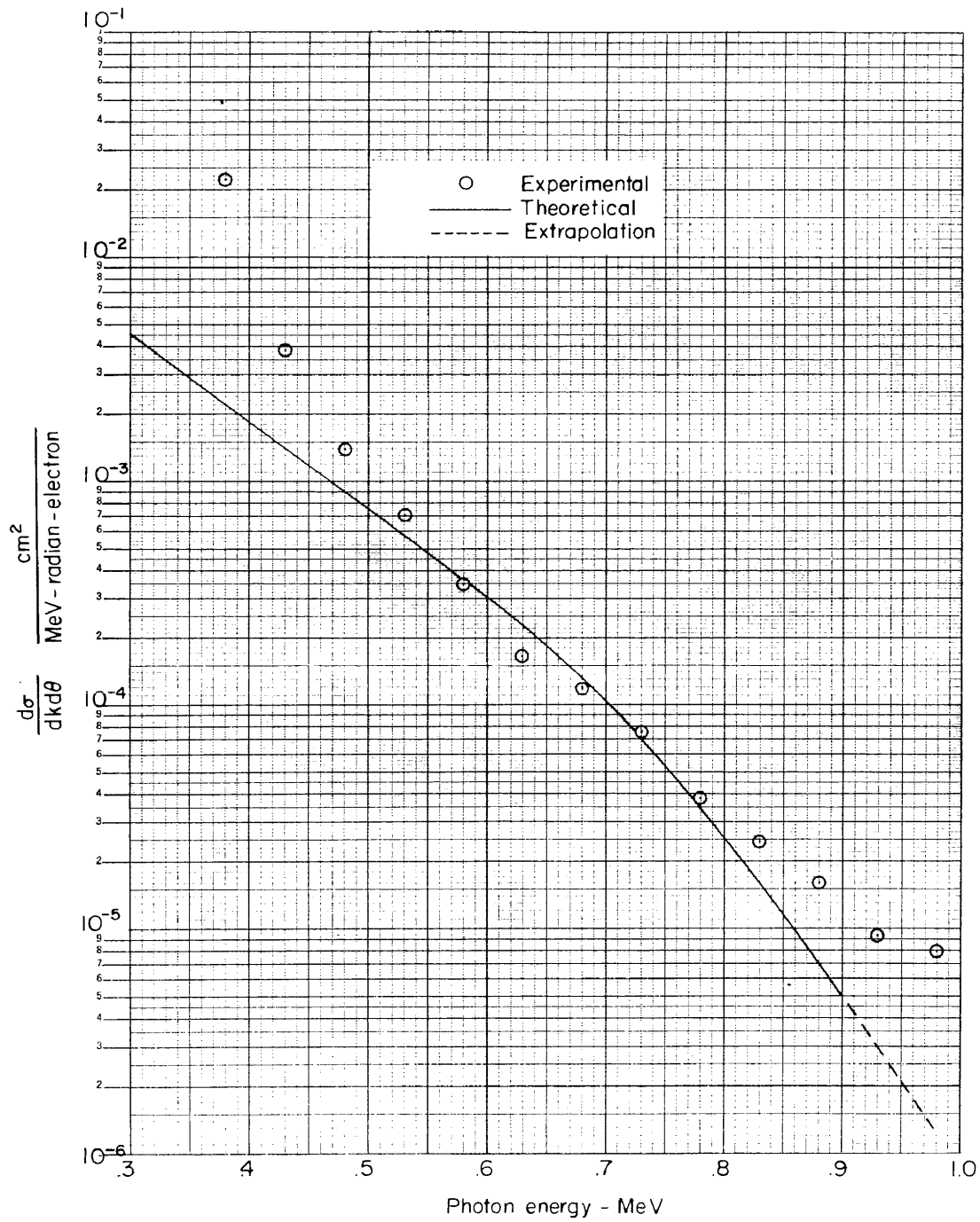
(g) $\theta = 105^\circ$.

Figure 12.- Continued.



(h) $\theta = 120^\circ$.

Figure 12.- Continued.



(i) $\theta = 135^\circ$.

Figure 12.- Concluded.

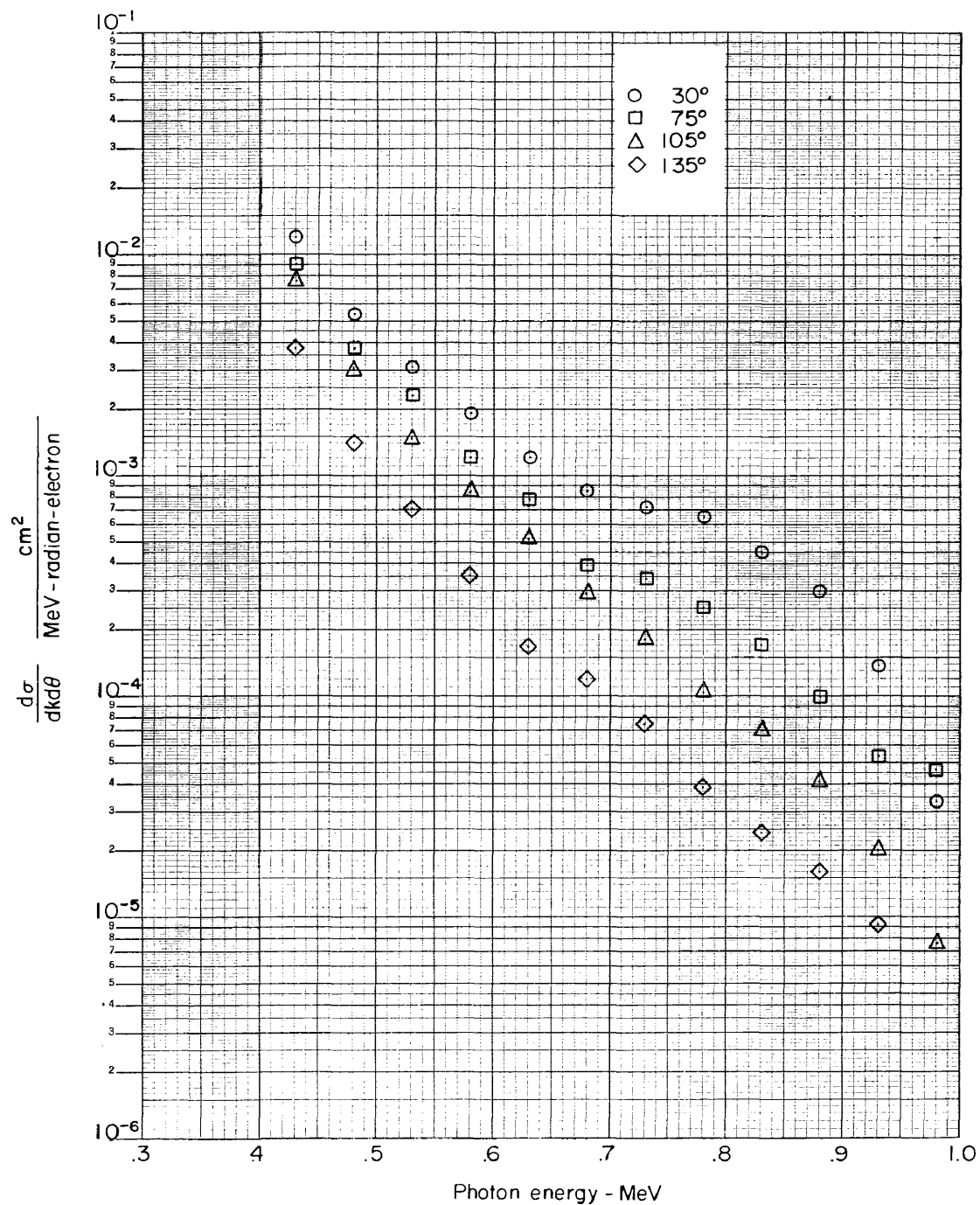


Figure 13.- Peaking of the bremsstrahlung cross section $\frac{d\sigma}{dk d\theta}$ in the forward direction. Incident electron energy $E_0 = 1.0$ MeV.

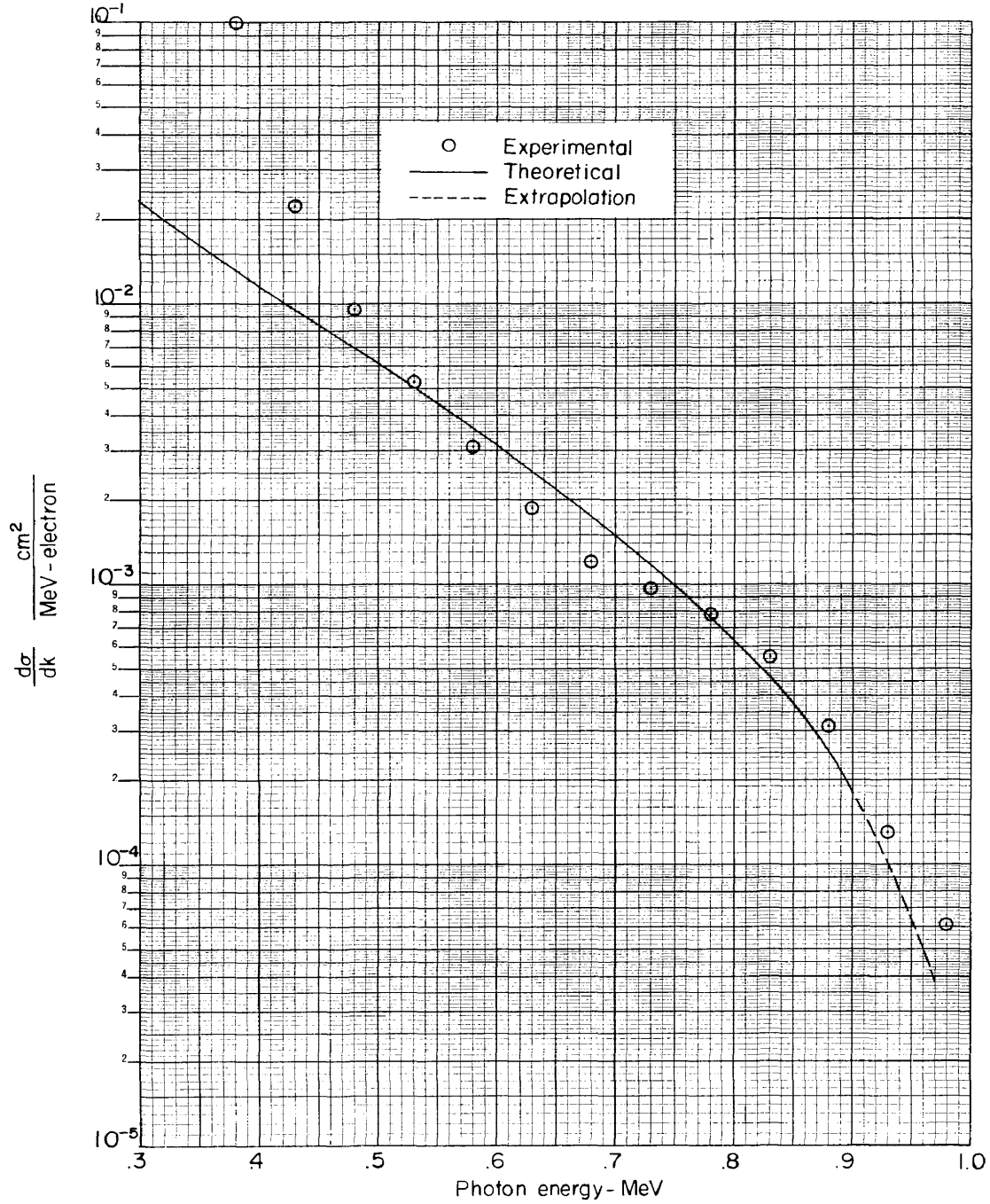


Figure 14.- Comparison of experimental bremsstrahlung cross section $\frac{d\sigma}{dk}$ with Born-approximation cross section. Incident electron energy $E_0 = 1.0$ MeV.